



# Substantial Biogeochemical and Biomolecular Processing of Dissolved Organic Matter in an Anticyclonic Eddy in the Northern South China Sea Down to Bathypelagic Depths

Miao Zhang<sup>1†</sup>, Siyu Li<sup>2†</sup>, Norbert Hertkorn<sup>2\*</sup>, Mourad Harir<sup>2,3</sup>, Dongfeng Xu<sup>4</sup>, Philippe Schmitt-Kopplin<sup>2,3</sup> and Ying Wu<sup>1\*</sup>

## OPEN ACCESS

### Edited by:

Toshi Nagata,  
The University of Tokyo, Japan

### Reviewed by:

Mario Uchimiya,  
University of Georgia, United States  
Liyang Yang,  
Fuzhou University, China

### \*Correspondence:

Ying Wu  
wuying@sklec.ecnu.edu.cn  
Norbert Hertkorn  
hertkorn@helmholtz-muenchen.de

<sup>†</sup>These authors have contributed  
equally to this work

### Specialty section:

This article was submitted to  
Marine Biogeochemistry,  
a section of the journal  
Frontiers in Marine Science

**Received:** 23 March 2022

**Accepted:** 28 April 2022

**Published:** 27 May 2022

### Citation:

Zhang M, Li S, Hertkorn N, Harir M,  
Xu D, Schmitt-Kopplin P and Wu Y  
(2022) Substantial Biogeochemical  
and Biomolecular Processing of  
Dissolved Organic Matter in an  
Anticyclonic Eddy in the Northern  
South China Sea Down to  
Bathypelagic Depths.  
*Front. Mar. Sci.* 9:902728.  
doi: 10.3389/fmars.2022.902728

<sup>1</sup> State Key Laboratory of Estuarine and Coastal Research, East China Normal University, Shanghai, China, <sup>2</sup> Helmholtz Zentrum Muenchen, German Research Center for Environmental Health, Research Unit Analytical Biogeochemistry (BGC), Neuherberg, Germany, <sup>3</sup> Chair of Analytical Food Chemistry, Technische Universitaet Muenchen, Freising-Weihenstephan, Germany, <sup>4</sup> State Key Laboratory of Satellite Ocean Environment Dynamics, Second Institute of Oceanography, Ministry of Natural Resources, Hangzhou, China

Solid-phase extracted dissolved organic matter (SPE-DOM) was isolated from two depth profiles at the core and at the edge of an anticyclonic eddy (ACE) in the northern South China Sea. Non-target nuclear magnetic resonance (NMR) spectroscopy and Fourier transform ion cyclotron mass spectrometry (FTICR/MS) of SPE-DOM revealed a higher uniformity of DOM molecules within the ACE than at the edge of the ACE. Small-scale upwelling of external nutrients may have contributed to higher productivity and production of fresher DOM, with higher proportions of CHNO and CHNOS compounds and low molecular weight species at the edge of the eddy. Common SPE-DOM molecules of supposedly biological origin such as carbohydrates and olefins were most abundant in the chlorophyll maximum layer in both stations. An unusual suite of ~10 abundant and ~35 less abundant tert-butyl benzene derivatives with potential to act as endocrine disruptors within a marine food chain and ~two dozen ketones of putative bacterial origin was recognized at meso- and bathypelagic depths in single-digit micromolar concentrations, with a distinct maximum at 1000 m depth at the edge of ACE. Downwelling might bring temporary large volumes of productive marine waters into deep waters, with micromolar concentration of abundant, microbial food web-specific metabolites (e.g. 2,4-di-tert-butylphenol et al.). In our study, these eventually added up to one quarter of common background biogeochemical marine organic matter even at bathypelagic depths and beneath and are significant food and energy sources for marine biota. Mesoscale chemical heterogeneity of marine water columns might extend to larger depths than currently anticipated and may create activity hotspots influencing biota, processing of DOM, and cycling of nutrients and trace elements.

**Keywords:** SPE-DOM, NMR, FTICR/MS, anticyclonic eddy, northern South China Sea

## INTRODUCTION

Marine dissolved organic matter (DOM) represents one of the largest pools of organic carbon on earth, comprises more than 90% of organic carbon in the ocean, and plays an essential role in the global carbon cycle. Molecular characterization of DOM will provide relevant information about its precursors (Hertkorn et al., 2013; Igarza et al., 2019), the biological and biochemical processes relating to DOM formation and degradation, including its reactive components (Gonsior et al., 2014; Padmavathi et al., 2014; Ali and Tremblay, 2019; Powers et al., 2019; Seidel et al., 2022), and might enable discrimination of biotic and abiotic processing of DOM in various ocean layers.

Ocean mesoscale eddies are ubiquitous in near coastal and open oceanic waters (McGillicuddy Jr, 2016), and strongly affect the transport of waters, abundance and biodiversity of marine organisms and marine DOM (Doblin et al., 2016; Sarma et al., 2019). Mesoscale eddies not only influence advective transport and vertical water mixing, but also affect biogeochemical cycles and the ocean biological pump (Garçon et al., 2001; McGillicuddy Jr, 2016; Siegel et al., 2011). In the northern hemisphere, most anticyclonic systems are oligotrophic, with nutrient-poor surface waters and restricted primary production. However, anticyclonic eddies (ACEs) are usually associated with relatively abundant microorganisms, an appreciable growth rate and DOC (dissolved organic carbon) accumulation (Bidigare et al., 2003; Ewart et al., 2008; Baltar et al., 2010), possibly triggered by downwelling in early-stage anticyclonic systems (Lasternas et al., 2012). DOC-rich surface waters and particulate organic carbon (POC) in ACEs were downwelled into deeper layers where extensive biogeochemical processing greatly affected its composition and the contributions of DOC to the oceanic carbon pump (Kolasinski et al., 2012; Lasternas et al., 2012). Intensification of ageostrophic secondary circulation produces small-scale hotspots of upwelling on the periphery of ACEs, which serve as a frontal zone between the eddy and the surrounding waters (Klein and Lapeyre, 2009; Siegel et al., 2011). As a result, both episodic nutrients and deep phytoplankton are driven upwards into euphotic zone, leading to the stimulation of primary production (PP) at the rim of anticyclonic eddies (Samuelson et al., 2012; Zhou et al., 2013; Wang et al., 2018).

The combination of optical spectroscopy with non-target nuclear magnetic resonance (NMR) spectroscopy and Fourier transform ion cyclotron resonance mass spectrometry (FTICR/MS) allows for an in-depth assessment of molecular diversity in marine and other DOM, which range among the most complex mixtures of organic molecules on earth (Hertkorn et al., 2007). This includes FTICR/MS-based assessment of heteroatoms CHNOS, distinction of chemical environments of hydrogen and carbon by NMR spectroscopy, and classification of chromophoric dissolved organic matter (CDOM) (Hertkorn et al., 2013; Hertkorn et al., 2016; Gonsior et al., 2017). Spectroscopic characterization of marine CDOM demonstrated a marked diversity between DOM in different water masses and allowed to distinguish putative sources of DOM (Kellerman et al., 2015; Wagner et al., 2015; Gonsior et al., 2017; Martínez-Pérez et al., 2017; Brogi et al., 2018). So far, only limited studies

have been carried out to decipher the chemical diversity of DOM in dynamic, upwelling and eddy marine systems; one example describes biotic and abiotic processing of DOM in the Peruvian upwelling system (Igarza et al., 2019).

The South China Sea (SCS) is the largest semi closed marginal sea between the Western Pacific and Eastern Indian Ocean, and mesoscale phenomena in SCS are ubiquitous (Xiang et al., 2016; Zhang et al., 2016; He et al., 2018), with a frequency of more than 30 per year including ~48% ACEs (Xiu et al., 2010). Wang et al. (2003) reported that most of the mesoscale eddies were distributed in the northern and eastern SCS, which modulated biogeochemical processes of SCS to remarkable extents.

To assess the impact of ACE on DOM composition and structure in SCS, two depth profiles of SPE-DOM from the edge and within an ACE from the northern SCS were isolated (**Figure 1**; **Table S1**), comprising samples obtained from surface (5 m), chlorophyll maximum zone (80-90 m), upper mesopelagic zone (200 m), mesopelagic zone (400-450 m), oxygen minimum zone (OMZ, 700-1000 m) with oxygen concentrations varying from 1.5-1.8 mg/L, deep layer (1400-1900m), with about 40-70% carbon yield. While effects of temporal isolation of water masses within ACE on microbial communities have been reported (Baltar et al., 2010; Fernández et al., 2008), we have determined bulk and spectroscopic parameters of these SPE-DOM samples with high spatial resolution to reveal whether temporal isolation of water masses within ACE will affect DOM composition and structure, in particular with regard to DOM at deeper waters. These data will allow a more comprehensive integration of mesoscale marine currents into the global carbon and other element cycles (e. g. N and S).

## MATERIALS AND METHODS

### Sampling

DOM samples were collected during March 2017 in the northern slope of SCS (**Figure 1**). An anticyclonic eddy born in January 2017, moving southwest was observed in the study area. Sampling points L05, L11 and L15 (from southwest to northeast) were across the eddy, with L05 and L15 on the edge and L11 in the center of the ACE (**Figure 1**). The downward contours of temperature, salinity and density ( $\sigma_t$ ) in L11 reflected the impact of downwelling of ACE in the upper layers (**Figure S1**).

Seawater for each sample was retrieved with acid-cleaned 12 L Niskin bottles attached to the CTD rosette, which recorded temperature, salinity,  $\sigma_t$ , chlorophyll fluorescence. Dissolved oxygen (DO) was measured immediately after sample collection with a DO analyzer (Jenco, San Diego, California, USA, Model 9173), which was calibrated with traditional iodometric method ( $r^2 = 0.9$ , slope = 0.97). Apparent oxygen utilization (AOU) was computed as the difference between oxygen saturation and the observed oxygen concentration (Garcia et al., 1992).

Seawater for DOM extraction was acidified to pH = 2 with HCl (Emsure, Merck) after filtration with GF/F glass filters

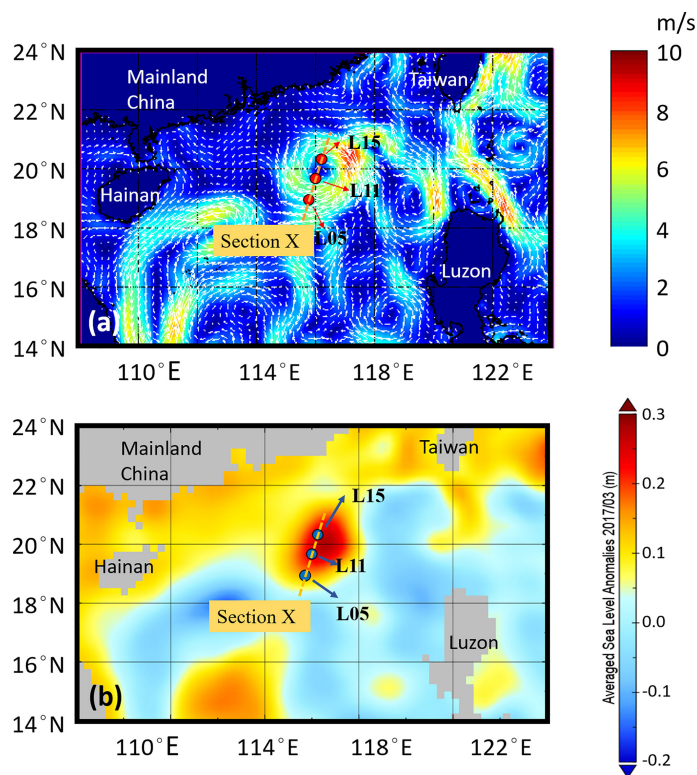


**FIGURE 1** | Map of sampling stations in Northern slope of South China Sea in March 2017. Depth profiles of SPE-DOM were obtained for stations L05 and L11. Chromophoric and fluorescent DOM were recorded in section X, including L05, L11 and L15. The color and vectors in **(A)** represented the velocity and direction of geostrophic flow. The color in **(B)** represents a sea level anomaly caused by ACE. This map was generated through combining SLA and surface geostrophic current velocity distributed by AVISO; <https://www.aviso.altimetry.fr>.

(Whatman, 0.7  $\mu\text{m}$  pore size; precombusted at 450°C for 5 h). A solid phase extraction (SPE) procedure was used to isolate DOM from the water with PPL cartridges (1 g, Agilent Bond Elut) as previously described (Dittmar et al., 2008). After conditioning of the cartridges with 10 mL methanol (GC-grade, Sigma-Aldrich) and Milli-Q water (pH = 2), 10 L acidified seawater for each sample were extracted with a cartridge. For removing the salt effect, the cartridges were rinsed with more than 20 mL Milli-Q water (pH = 2) and stored at -20°C in the dark until analyses. Before measurement, the cartridges were dried by flushing with high purity  $\text{N}_2$  and eluted with methanol (GC-grade, Sigma-Aldrich). The recovery of SPE-DOM ranged from 40-70% (**Table S1**).

## NMR Spectroscopy

For NMR spectroscopy, aliquots of original methanol solutions of marine SPE-DOM samples were evaporated in vacuo to dryness and deuterated methanol ( $\text{CD}_3\text{OD}$ ) was added; this cycle was repeated three times to largely exchange methanol- $\text{h}_4$  with methanol- $\text{d}_4$ . Here, ~1-3.5 mg yellow solid marine SPE-DOM was obtained. The  $^1\text{H}$  NMR spectra of all the South China Sea SPE-DOM samples were acquired with a Bruker Advance III NMR spectrometer operating at 800.35 MHz ( $B_0 = 18.8$  Tesla) and Topspin 3.5.7 software with samples from redissolved solids

in sealed 2.0 mm Bruker Match tubes. Proton detected NMR spectra were acquired at 283 K with an inverse geometry 5 mm z-gradient  $^1\text{H}/^{13}\text{C}/^{15}\text{N}/^{31}\text{P}$  QCI cryogenic probe (quaternary cryogenic inverse; 90° excitation pulses:  $^{13}\text{C} \sim ^1\text{H} \sim 10 \mu\text{s}$ ). NMR chemical reference:  $^1\text{H}/^{13}\text{C}$  NMR,  $\text{CD}_3\text{OD}$ : 3.30/49 ppm. 1-D  $^1\text{H}$  NMR spectra were recorded with a spin-echo sequence (10  $\mu\text{s}$  delay) to allow for high-Q probe ring-down (Q: high quality factor), and classical presaturation to attenuate residual water present: *noesypr1d*, typically 512-2048 scans (5 s acquisition time, 5 s relaxation delay (d1), 1 ms mixing time; 1 Hz exponential line broadening). Absolute value J-resolved (JRES), COSY and phase-sensitive TOCSY/NOESY NMR spectra (correlation spectroscopy; total correlated spectroscopy, nuclear Overhauser spectroscopy) used acquisition times of 1 s at a spectral width of 9615 Hz, with 50 Hz sweep with in F1 (JRES), 70 ms dipsi-2 mixing sequence (TOCSY with solvent suppression: *dipsi2etgpsi19*); NOESY mixing time 350 ms (*noesygp2pph*). Carbon decoupled  $^1\text{H}$ ,  $^{13}\text{C}$  HSQC spectra (heteronuclear single quantum coherence; *hsqcedetgpsi2.2*) were acquired under the following conditions: acquisition time: 250 ms;  $^{13}\text{C}$  90° decoupling pulse, GARP (70  $\mu\text{s}$ ); 50 kHz WURST 180°  $^{13}\text{C}$  inversion pulse (wideband, uniform, rate, and smooth truncation; 1.2 ms); F2 ( $^1\text{H}$ ): spectral width (SW) of 9615 Hz,  $^1J_{\text{CH}} = 150$  Hz, 1.25 s relaxation delay; F1 ( $^{13}\text{C}$ ): SW =

33784 Hz (167.9 ppm); number of scans (F2)/F1-increments ( $^{13}\text{C}$  frequency) for SPE-DOM (400–1800/137–142). HMBC spectra (heteronuclear multiple bond coherence; *hmbcabcigplnd*) were acquired with  $aq = 1$  s,  $d1 = 0.5$  s, F1 ( $^{13}\text{C}$ ): SW = 52083 Hz (258.8 ppm).  $^{13}\text{C}$  NMR spectra were acquired with a Bruker Advance III NMR spectrometer operating at 500.13 MHz ( $B_0 = 11.7$  T) and used inverse gated WALTZ-16 decoupling (wideband alternating-phase low-power technique for zero residual splitting; 19 s relaxation delay; with an acquisition time ( $aq$ ) of 1 s;  $^{13}\text{C}$  DEPT NMR spectra used  $aq = 1$  s and  $d1 = 2$  s; the one bond coupling constant  $1J(\text{CH})$  was 150 Hz; exponential line broadening was  $lb = 12.5$  Hz. Other acquisition conditions are provided in **Table S2**. Compound M2\* (3-(3,5-Di-tert-butylphenyl) propionic acid was purchased from Abcr GmbH, Karlsruhe, Germany, and dissolved as provided in  $\text{CD}_3\text{OD}$  for acquisition of NMR spectra.

## FTICR/MS Analysis

Negative electrospray ionization [(-)ESI] Fourier transform ion cyclotron resonance mass spectra (FTICR/MS) were acquired using a 12 T Bruker Solarix mass spectrometer (Bruker Daltonics, Bremen, Germany) and an Apollo II electrospray ionization source in negative mode. Nebulizer gas pressure, drying gas pressure and the source heater temperature were 138 kPa, 103 kPa and 200°C, respectively. The spectra were acquired with a time domain of 4 MW and 300 scans were accumulated for each mass spectrum. Computation of elemental formulas for each peak was done in a batch mode by an in-house written software tool. The generated formulae were validated by setting sensible chemical constraints (N rule, O/C ratio  $\leq 1$ , H/C ratio  $\leq 2n + 2$  ( $\text{C}_n\text{H}_{2n+2}$ ), element counts:  $\text{C} \leq 100$ ,  $\text{H} \leq 200$ ,  $\text{O} \leq 80$ ,  $\text{N} \leq 3$ ,  $\text{S} \leq 2$ ,  $\text{P} < 1$  and mass accuracy window, set at  $\pm 0.5$  ppm). Final formulae were generated and categorized into groups containing CHO, CHNO, CHOS or CHNOS molecular

compositions, which were used to reconstruct the group-selective mass spectra (Schmitt-Kopplin et al., 2010a; Schmitt-Kopplin et al., 2010b). The computed average values for H, C, N, O and S (atom %), elemental ratios, DBE-related parameters and average mass ( $m/z$ ) given in **Table 1** were based upon intensity-weighted averages of area-normalized mass spectra using assigned molecular formulae.

Compounds were classified based on elemental stoichiometries (H/C and O/C ratios) and a modified aromaticity index ( $\text{AI}_{\text{mod}}$ ) (Koch and Dittmar, 2006; Ohno et al., 2010; Šantl-Temkiv et al., 2013; Wagner et al., 2015; Igarza et al., 2019), which allocated condensed compounds ( $\text{AI}_{\text{mod}} \geq 0.67$ ), highly unsaturated compounds ( $\text{AI}_{\text{mod}} < 0.50$ ,  $\text{H/C} < 1.5$ ,  $\text{O/C} < 0.9$ ), unsaturated compounds ( $1.5 \leq \text{H/C} \leq 2.0$ ,  $\text{O/C} < 0.9$ ), peptide-like compounds ( $1.5 \leq \text{H/C} \leq 2.0$ ,  $\text{O/C} < 0.9$ ,  $\text{N/C} > 0$ ), saturated compounds ( $\text{H/C} > 2.0$ ,  $\text{O/C} < 0.9$ ), and carbohydrate-like compounds ( $1.5 \leq \text{H/C} \leq 2.0$ ;  $\text{O/C} \geq 0.9$ ). Mass spectrometry data did not allow discrimination of isomeric structures.

## Statistical Analysis

Hierarchical Cluster Analysis (HCA) was performed based on 0.01 ppm buckets of  $^1\text{H}$  NMR spectra (from 0.5–10 ppm, with exclusion of HDO and  $\text{CD}_2\text{HOD}$ ) and assigned, intensity-weighted mass peaks ( $n = 7960$ ) in FTICR mass spectra, using the Hierarchical Clustering Explorer 3.0 (HCE; <http://www.cs.umd.edu/hcil/multi-cluster/>), with clustering of the dataset using the Average Linkage (UPGMA) method and the Pearson correlation coefficient (Pearson's R) as the similarity/distance measure. Based on the HCA, we used the "profile search" tool from HCE 3.0, choosing a search method (model-based), a distance measure (Pearson's R) and a threshold (0.9). Principal Component Analysis (PCA) was done with the software SIMCA-P 9.0 (Umetrics AB, Sweden). FTICR mass spectra were arranged

**TABLE 1** | Counts of mass peaks and FTICR/MS-derived bulk parameters as computed from negative electrospray (ESI) 12 T FTICR mass spectra for singly charged ions.

Members of molecular series	L05 5m	L05 80m	L05 200m	L05 400m	L05 1000m	L05 1898m	L11 5m	L11 90m	L11 200m	L11 450m	L11 700m	L11 1490m
CHO compounds	1444	1163	1797	1439	1593	1579	1519	1812	1553	1341	1359	1210
	41.0%	42.5%	43.8%	40.6%	44.4%	40.0%	40.1%	40.3%	40.9%	41.6%	43.7%	43.0%
CHOS compounds	579	373	489	592	459	563	588	611	622	467	522	481
	16.4%	13.6%	11.9%	16.7%	12.8%	14.3%	15.5%	13.6%	16.4%	14.5%	16.8%	17.1%
CHNO compounds	1269	1113	1647	1365	1383	1618	1500	1854	1450	1299	1074	1020
	36.1%	40.7%	40.1%	38.5%	38.6%	41.0%	39.6%	41.2%	38.2%	40.3%	34.6%	36.2%
CHNOS compounds	228	85	172	151	151	187	182	224	172	115	152	105
	6.5%	3.1%	4.2%	4.3%	4.2%	4.7%	4.8%	5.0%	4.5%	3.6%	4.9%	3.7%
Number of assigned mass peaks	3520	2734	4105	3547	3586	3947	3789	4501	3797	3222	3107	2816
average H [%]	44.41	44.47	44.5	44.5	44.49	44.77	44.46	44.68	44.25	44.19	44.47	44.17
average C [%]	36.23	36.22	36.46	36.52	36.83	36.86	36.27	36.15	36.38	36.57	36.79	36.90
average O [%]	18.25	18.48	18.13	17.96	17.78	17.25	18.29	18.19	18.46	18.29	17.64	18.05
average N [%]	0.84	0.67	0.71	0.75	0.69	0.89	0.74	0.75	0.65	0.71	0.75	0.60
average S [%]	0.27	0.17	0.21	0.27	0.21	0.23	0.25	0.24	0.25	0.23	0.35	0.28
computed average H/C ratio	1.23	1.23	1.22	1.22	1.21	1.21	1.23	1.24	1.22	1.21	1.21	1.20
computed average O/C ratio	0.50	0.51	0.50	0.49	0.48	0.47	0.50	0.50	0.51	0.50	0.48	0.49
computed average C/N ratio	43.2	54.0	51.6	48.8	53.5	41.3	49.3	48.3	55.6	51.7	49.2	61.2
computed average C/S ratio	134	211	177	138	173	160	145	154	145	157	104	134
average DBE	7.8	7.7	8.2	8.1	8	9	7.8	7.9	8	8	7.8	8
average DBE/C	0.42	0.42	0.42	0.43	0.43	0.43	0.42	0.42	0.43	0.43	0.43	0.44
mass weighted average (Da)	403.7	397.6	416.8	411.8	399.1	450.9	405.6	414.7	409.8	401.4	388.9	396.8

with the samples as observations and the peak areas of the assigned FTICR mass peaks as the response variables.  $^1\text{H}$  NMR spectra were arranged with the samples as observations and the NMR resonances as the response variables (800 MHz  $^1\text{H}$  NMR,  $\text{CD}_3\text{OD}$ , area-normalized from 0.5-10.0 ppm; 0.01 ppm bucket resolution; with the exclusion of residual water and methanol NMR resonances). Before multivariate statistics were performed, the response variables were centered and scaled to unit variance. The based weight was computed as  $1/\text{sqrt}$  (standard deviation of the response variables). SPSS 23.0 was used to compute the correlation between assigned molecular series and optical parameters (Spearman's R) within 0.95 confidence limit.

## RESULTS AND DISCUSSION

### Chemical Diversity of SPE-DOM in SCS

The proton NMR spectra of the SPE-DOM samples in SCS showed smooth, broad bulk envelopes familiar from highly processed biogeochemical marine DOM that represent

superpositions of millions of atomic environments grouped in key substructures (**Figures 2, S2–S4**) (Hertkorn et al., 2013). In general, the abundance of sharp resonances in  $^1\text{H}$  NMR spectra declined in the order of  $\text{L05}_{1000\text{m}} \approx \text{L11}_{700\text{m}} > \text{L05}_{400\text{m}} \approx \text{L11}_{450\text{m}} \approx \text{L05}_{1898\text{m}} \approx \text{L11}_{1490\text{m}} > \text{L05}_{200\text{m}} \approx \text{L11}_{200\text{m}} \approx \text{L05}_{80\text{m}} \approx \text{L11}_{90\text{m}} \approx 5\text{ m}$ . This was in stark contrast with the supposed large extent of biological activity and primary production in the near surface ocean photic zone ( $< 200\text{ m}$ ), and the supposedly low microbial production in the oxygen minimum zones  $\text{L05}_{1000\text{m}}$  and  $\text{L11}_{700\text{m}}$  (**Figures 2, S2–S4**) (Arnosti, 2011) (for further description, cf. Metabolites and Biogeochemical Organic Matter in ACE of SCS). From higher to lower field (from right to left), key substructures such as abundant aliphatic ( $\text{CCCH}$  units;  $\delta_{\text{H}} \sim 0.5\text{--}1.9\text{ ppm}$ ), “acetate and acetyl-analogue” ( $\text{H}_3\text{C-C(=O)-Z}$ ;  $\delta_{\text{H}} \sim 1.9\text{--}2.0\text{ ppm}$ ), remotely functionalized oxygenated ( $\text{OCCH}$  units including carboxyl-rich alicyclic molecules (CRAM;  $\delta_{\text{H}} \sim 2.0\text{--}3.1\text{ ppm}$ ), oxygenated aliphatic ( $\text{OCH}$  units, including carbohydrate-like and methoxy ( $\text{H}_3\text{CO}$ ) units ( $\delta_{\text{H}} \sim 3.1\text{--}4.9\text{ ppm}$ ), olefins ( $-\text{C}=\text{CH}$ ) ( $\delta_{\text{H}} \sim 5.0\text{--}7.0\text{ ppm}$ ), and aromatic ( $\text{C}_{\text{ar}}\text{H}$ ) units ( $\delta_{\text{H}} \sim 7.0\text{--}10.0$

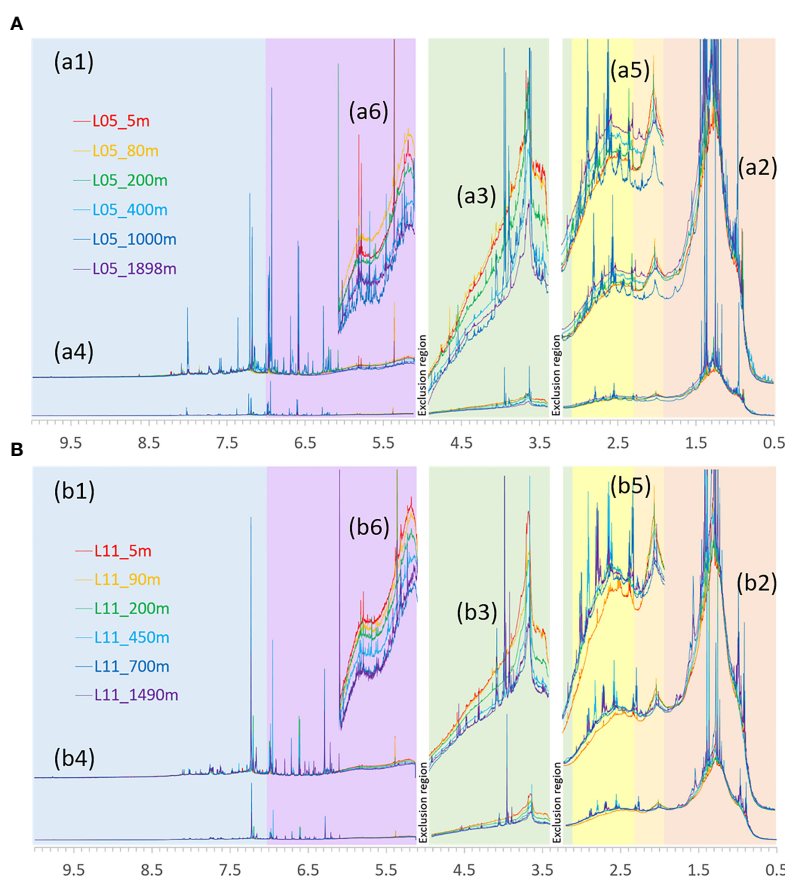


**FIGURE 2 | (A)** Area normalized  $^1\text{H}$  NMR spectra (800 MHz,  $\text{CD}_3\text{OD}$ ) of SPE-DOM for depth profiles of **(A)** L05 (a1–a6) and **(B)** L11 (b1–b6) in which the total NMR resonance area equals 100%, from  $\delta_{\text{H}} = 0.5\text{--}10.0\text{ ppm}$ , with exclusion of residual water and methanol NMR resonances. (a1, b1) Entire NMR spectrum ( $\delta_{\text{H}} = 0.5\text{--}10.0\text{ ppm}$ ); (a2, b2) vertical expansion of aliphatic protons,  $\delta_{\text{H}} \sim 0.5\text{--}3.1\text{ ppm}$ ; (a3, b3) vertical expansion of HC-O protons,  $\delta_{\text{H}} \sim 3.4\text{--}4.8\text{ ppm}$ ; (a4, b4) section of unsaturated protons,  $\delta_{\text{H}} > 5\text{ ppm}$ ; (a5, b5) vertical expansion of functionalized aliphatic compounds, associated also with carboxyl-rich alicyclic compounds (CRAM); (a6, b6) vertical expansion of olefins,  $\delta_{\text{H}} \sim 5.1\text{--}6.1\text{ ppm}$ .

ppm)  $^1\text{H}$  NMR resonances showed clearly recognizable and rather broad maxima (**Figures 2, S2, S3**). In L05 and L11 SPE-DOM samples, superimposed sharp NMR resonances representing biological molecules appeared most prominent in unsaturated protons ( $C_{sp2}\text{H}$ ;  $\delta_{\text{H}} > 5.0$  ppm), but were also clearly discernible in the section of aliphatic protons ( $\text{OCH}$  and  $\text{CCH}$  chemical environments; **Figures 2, S2, S3**).  $^1\text{H}$  NMR spectra visibly differed with depth, and the variance among profile layers referred mainly to intensity (denoting variable abundance of key substructures) rather than positioning of resonances (denoting molecular diversity) (**Figures 2, S2, S3**). Massive projection of millions of individual atomic environments of  $^1\text{H}$  atoms produces sweeping intrinsic averaging in NMR spectra of SCS organic matter (Hertkorn et al., 2007), and extensive molecular changes are required to produce visible differences of bulk NMR spectral features, which reflect multiple layers of biogeochemical processing in marine foodwebs. In comparison, the chemical diversity of biomolecules from known metabolic networks is more limited than that of biogeochemical molecules like DOM. Recognizable biomolecules in marine SPE-DOM are typically much more abundant than (non-assigned and largely unknown) individual biogeochemical molecules ( $\sim 10^{-4}$  compared with  $\leq 10^{-7}$  of  $^1\text{H}$  NMR integral); they share common structural features (Hoffmann et al., 2020) and project on narrow ranges of  $^1\text{H}$  NMR chemical shift. Hence, even minor operating biochemical processes will produce readily recognizable features in  $^1\text{H}$  NMR spectra of marine SPE-DOM.

The differences between  $^1\text{H}$  NMR spectra of each sampling depth indicated various physical and biochemical processes in different layers (**Figures 2, S2–S4**). While many methyl resonances terminating alkyl groups resonated near  $\delta_{\text{H}} \sim 0.9$  ppm, the resonances of upper layer ( $< 200$  m) for L05 and L11 were more smooth than those of deep layers ( $> 400$  m) (**Figures 2-a2, b2**). Similarly, the intensity maxima at  $\delta_{\text{H}} \sim 1.3$  ppm at deep water layers, representing methylene, alkyls and other purely aliphatics with  $\text{HC} \geq 4$  bonds away from the next heteroatoms, were higher than those in upper layers (**Figures 2-a1, b1**). Combined with the progressively increasing downfield shoulders ranging  $\delta_{\text{H}} \sim 1.4$ – $1.7$  ppm, which represented certain remotely oxygenated aliphatics and alicyclic rings (**Figures 2-a2, b2**), higher proportions of aliphatic protons ( $\delta_{\text{H}} \sim 0.5$ – $1.9$  ppm) were observed in the deep layers rather than in the upper layers (**Figure S4**). The resonances coincident with acetyl and acetate derivatives ( $\delta_{\text{H}} \sim 2.1$  ppm) decreased from surface to OMZ, and then increased slightly (**Figures 2-a5, b5**). Functionalized aliphatics including those with remote carboxylic substitution typical of CRAM (heteroatoms  $\geq 2$  bonds away from protons;  $\delta_{\text{H}} \sim 2.3$ – $3.1$  ppm) increased from surface to bottom, except SPE-DOM of L05\_1000 m which showed comparatively low abundance of these units (**Figure S4**). The superimposed small NMR resonances indicating the diversity of CRAM protons and related biomolecules were more significant in deep layer ( $> 400$  m) (**Figures 2-a5, b5**). Isolated double bonds ( $\delta_{\text{H}} \sim 5.2$ – $6.0$  ppm) were characteristic of natural products (Pisani et al., 2018), and commonly declined from surface to depth, in the order of  $80\text{ m} > 5\text{ m} > 200\text{ m} > 400\text{ m} \sim 1898\text{ m} > 1000\text{ m}$  in L05 station and  $5\text{ m} > 90\text{ m} > 200\text{ m} > 450\text{ m} > 700\text{ m} \sim 1490\text{ m}$  in L11 station

(**Figures 2-a6, b6**). Oxygenated aliphatic ( $\text{OCH}$ ) units also decreased from surface to deep waters (**Figure S4**) (Hertkorn et al., 2013; Benner and Amon, 2015).

The relative abundance of pure aliphatic protons ( $\text{HC-C-C-}$ ;  $\delta_{\text{H}} \sim 0.5$ – $1.9$  ppm) in marine DOM always exceeded 40%, with higher abundance in deep ( $\sim 48\%$ ) than in surface ( $\sim 42\%$ ) waters (**Figure S4**). In both L05 and L11, the relative abundance of the functionalized protons ( $\text{HC-N}$ ,  $\text{HC-C-O}$ ;  $\delta_{\text{H}} \sim 1.9$ – $3.1$  ppm) increased from surface to bottom layers. In OMZ (1000 m of L05, 700 m of L11), however, the relative abundance of functionalized protons decreased slightly. The abundance of carbohydrates, alcohols, esters, ethers and other singly oxygenated units ( $\text{HCO}$ ;  $\delta_{\text{H}} \sim 3.1$ – $5.0$  ppm) at L05 and L11 stations declined from surface to deep (**Figure S4**), and more strongly in the upper 200 m, demonstrating that oxygenated aliphatic molecules were produced primarily within the sunlit layer of the surface ocean and consumed primarily within the upper mesopelagic zone (Benner and Amon, 2015).

The total contributions of aliphatic  $\text{HC-C-C-}$ ,  $\text{HC-N}$ ,  $\text{HC-C-O}$  and  $\text{HCO}$  units were higher than 90% in marine SPE-DOM. Olefins ( $\text{HC=C-}$ ;  $\delta_{\text{H}} \sim 5.0$ – $7.0$  ppm) and aromatics ( $\text{H}_{\text{ar}}$ ;  $\delta_{\text{H}} \sim 7.0$ – $10.0$  ppm) contributed to the unsaturated protons, with  $< 10\%$  of total  $^1\text{H}$  NMR integral and slight variance in the water profile (**Figure S4**). The relative abundance of olefinic protons in upper layers was higher than that in the deep layers, in line with the supposed biological origin of olefins ( $\text{HC} = \text{C}$ , some anomeric positions  $\text{HCO}_2$  of supposedly biotic origin also resonated here) (Hertkorn et al., 2013; Pisani et al., 2018), (**Figure S4**). In the OMZ of L05, however, the olefins were also abundant (**Figure 2**).

The content of aromatic proton ( $C_{\text{ar}}\text{H}$ ) was highest in the OMZ, which could result from the decreased activity of microbes when lacking oxygen. The ratio between olefinic and aromatic protons ( $H_{\text{olefinic}}/H_{\text{aromatic}}$ ) varied between 1.7 and 2.8, indicating that the relative abundance of olefinic protons exceeded that of aromatic protons in marine SPE-DOM, in accordance with previous results (Hertkorn et al., 2013). The ratio  $H_{\text{olefinic}}/H_{\text{aromatic}}$  was highest in the chlorophyll maximum layer and lowest in the OMZ (**Figure S4**), indicative of a production of olefins and aromatic substances by different biochemical processes in marine water profiles. Ratios of aliphatic to aromatic protons ( $H_{\text{aliphatic}}/H_{\text{aromatic}}$ ) were lowest in OMZ of both stations, suggesting the decline of microbial-derived aliphatic rich DOC (Hertkorn et al., 2016).

FTICR mass spectrometry with negative electrospray ionization of SCS SPE-DOM provided several thousands of mass peaks (**Figure S5**), of which many hundreds could be assigned to extended CHO, CHOS, CHNO, and CHNOS molecular series (**Table 1; Figure S5**) based on excellent mass accuracy and mass resolution (Hertkorn et al., 2008; Schmitt-Kopplin et al., 2010b). In the upper 200 m, higher numbers of molecular formulas were assigned in L11 than in L05, while more mass peaks were assigned in the deep layer for L05 than for L11 samples (**Table 1**).

Visual inspection of the spectra showed smooth, slightly skewed near Gaussian distributions of mass peaks, with

prominent mass spacings caused by  $\pm \text{CH}_2$  ( $\Delta m = 14.0565$  Da) and  $\pm \text{H}_2$  ( $\Delta m = 2.00121$  Da), accompanied by sets of abundant low mass peaks with declining relative abundance in the order  $L11_{700\text{ m}} \approx L05_{1000\text{ m}} > L11_{1490\text{ m}} \approx L05_{200\text{ m}} > L11_{90\text{ m}} \approx L11_{5\text{ m}}$  (**Figure S5**); these irregular series often represent relatively abundant biomolecules, but also impurities like pollutants or surfactants might have contributed. No clear mass shift of the most abundant mass peaks was observed, but a relative depletion of low mass peaks from top to bottom layers in L05 and less so in L11 took place ( $m/z < 350$ ; **Figure S5**), reflecting progressive degradation of low  $m/z$  molecules along the depth profile (Flerus et al., 2012; Hertkorn et al., 2013). The OMZ at  $L05_{1000\text{ m}}$  and  $L11_{700\text{ m}}$  showed the lowest average mass (**Table 1**; **Figure S5**).

The FTICR/MS-derived relative weight percentage of oxygen in SPE-DOM decreased slightly from surface to deep layers in station L05 and showed no obvious trend in station L11 (**Table 1**). Meanwhile, the weight percentage of carbon increased from surface to deep, and hence, the computed O/C ratio decreased steadily from upper to deep layers, probably caused by a combination of abiotic (e.g. redox chemistry, photochemistry, mineral association) and biotic processes (e.g. metabolism of organisms in foodwebs, lysis and exudation) subject to upwelling/downwelling propagation, resulting in less oxygenated (i.e. defunctionalized) organic matter following loss of  $\text{H}_2\text{O}$  and  $\text{CO}_2$  upon processing, which then might become less degradable and acts as carbon sink in the ocean (**Table 1**) (Nebbioso and Piccolo, 2013). The average H/C ratio very slightly decreased from surface ( $\sim 1.23$ ) to bottom waters ( $\sim 1.20$ ) in L05 and L11. The total weight percentage of assigned nitrogen and sulfur in organic compounds was  $< 1\%$  in the water profile. CHO-molecular series comprised  $> 40\%$  in all SCS SPE-DOM, with a relative maximum at the OMZ for both stations (44.4% of L05 and 43.7% of L11, respectively), and the count of CHO compounds increased from surface to bottom in L05 but decreased in L11. CHNO-molecular series were the second most abundant compounds in SCS SPE-DOM, with contributions of 35–41% to total assigned molecules. The relative proportions of both CHO and CHNO molecular series increased with depth in L05 and decreased in L11, and the highest percentage of CHNO compounds was observed in the chlorophyll maximum zone of both stations. The contributions of assigned CHOS- and CHNOS-molecular series were about 20% with less variation in the water profiles. Double Bond Equivalent (DBE), an empirical criterion to provide counts of C=C and C=O double bonds as well as numbers of alicyclic rings present in molecular compositions and DBE per carbon (DBE/C) were proposed for identification of (condensed) aromatic structures from FTICR mass spectra (Koch and Dittmar, 2006). DBE/C in SPE-DOM increased from surface to deep (**Table 1**), in line with previous studies (Benner et al., 1992; Flerus et al., 2012; Repeta, 2015), reflecting a progressive increase of relative unsaturation in deep water DOM, which may impart some resistance to microbial degradation of “residual” DOM.

The highly unsaturated compounds (HU; for definition, see methods) contributed most to the SCS SPE-DOM (86.2%) (**Figure S6**; **Table S3**), and was higher than in the Pacific

ocean (Igarza et al., 2019). HU showed highest average molecular weight and largely comprised CHO compounds. The relative abundance of HU increased from surface to deep waters, but was lowest in the OMZ (**Table S3**). The unsaturated compounds (UC) represented 9.5% of SPE-DOM, including 2.4% of peptide-like molecular series. Although no sulfur or nitrogen atoms were present in more than 74% of UC, the percentage of S-containing molecular series was higher than that in HU (**Figure S6**). The UC molecular series decreased with depth except at the OMZ, in which more UC were observed. UC in the chlorophyll a maximum zone was slightly more abundant in L11 (11.7%) than in L05 (10.5%) (**Table S3**). The average molecular weight of CHNO compounds (418 Da) was higher than other UC, which decreased from surface to deep. Meanwhile, more CHNO compounds were present in L11 chlorophyll a maximum zone than at L05 (**Table S3**). The MS-based percentages of condensed compounds (CC), saturated compounds (SC) and sugars-like molecular series were less than 1% respectively (**Figure S6**). More than half of condensed molecular series had no sulfur atom, while most contained one or more nitrogen atom (**Figure S6**), also shown in van Krevelen diagrams (**Figure S7**). The percentage of CC in chlorophyll a maximum zone of L05 was much lower than others, indicating that fresher DOM was produced (**Table S3**). The average molecular weight of SC was lowest (343 Da), most of which contained one sulfur atom (**Figure S6**). The distribution of SC in L05 and L11 was reversed (**Table S3**). About 80% of carbohydrate-like compounds had one or more nitrogen, only 20%, however, were sulfur-bearing (**Figure S6**). In chlorophyll a maximum zone, sugars-like compounds were more abundant in L05 than L11, congruent with NMR results.

In L05 and L11, CHO and CHNO compounds formed contiguous lobes in van Krevelen and mass-edited H/C ratio diagrams, whereas CHOS compounds formed single contiguous lobes in mass-edited H/C diagrams and two distinct lobes in van Krevelen diagrams, indicative of two different classes of CHOS compounds being present in L05 and L11 SPE-DOM (**Figure S7**). The CHOS and CHNOS compounds with high H/C and O/C ratios progressively decreased with water depth (**Figure S7**). CHNOS compounds were more scattered in all these diagrams, with a minor contiguous lobe ( $\text{H/C} \sim 1.0 - 1.6$ ;  $\text{O/C} \sim 0.45 - 0.7$ ) in van Krevelen diagrams of L11 (**Figure S7**). Contiguous lobes are indicative of processed biogeochemical materials, with a steep decline of relative abundance at the edges that originate from intrinsic averaging in extremely complex mixtures of organic molecules (Hertkorn et al., 2007). In comparison, scatter typically results from a less deep coverage of the compositional space; this applies here as well because CHNOS compounds were much fewer than the other molecular series (**Table 1**). Considering, that entropy-driven biogeochemical processing of organic matter frequently results in continual distributions of bulk properties, with strong gradients toward the edge, the conspicuous scatter of CHNOS compounds in both van Krevelen and mass-edited H/C diagrams at first is in line with the lower relative counts and abundance (**Table 1**) but also testifies for significant contributions of biological processes in their formation (Hertkorn et al., 2016). The CHO compounds in

FTICR/MS-derived van Krevelen diagrams of L05 and L11 were positioned in accordance with CRAM ( $O/C = 0.3-0.6$ ,  $H/C = 0.7-1.6$ ; (Hertkorn et al., 2006)) (Figures S7-e1, e5). CHNO compounds occupied larger areas than CHO compounds in van Krevelen diagrams and mass-edited H/C ratios (Figure S7), indicative of a larger chemical diversity (Andersson et al., 2019) for CHNO compounds of yet unknown provenance, with more saturated ( $H/C > 1.6$ ) and more oxygenated ( $O/C > 0.8$ ) molecules than observed in CHO compounds. Highly oxygenated CHNO compounds ( $O/C > 0.7$ ), which were more abundant in the upper than in the deep layers, showed higher relative saturation ( $H/C > 1.2$ ) than the other CHNO compounds and possibly comprised polyoxygenated aliphatic compounds with N-containing functional groups of yet unknown provenance. The assigned CHOS molecular series showed appreciable unsaturation, with H/C ratios ranging from 1.0-1.4 (Figure S7), and less ( $O/C < 0.4$ ) and more oxygenated ( $O/C > 0.4$ ) compounds (Figure S7) resulted from different biogeochemical processes. In the upper layers of L05 (5 m and 80 m), S-bearing polyoxygenated compounds were present (Figures S7-b, S7-a2, b2, section b), which were not obvious in L11; these were probably related to primary production at the edge of ACE. Higher proportions of less oxygenated CHOS molecular series were observed in the deep layer of L05 (Figure S7-f2, section c).

## Spatial Discrimination of SPE-DOM in the ACE

Nutrients when supplied to the upper layers with the small-scale upwelling at the edge of ACE might stimulate primary production, with synthesis of rather fresh organic matter (Samuelson et al., 2012; Karstensen et al., 2017). NMR and FTICR mass spectra were supportive of biotic process participating in the formation of DOM. When the  $^1H$  NMR spectral intensities were scaled to 100% total integral within the entire region of chemical shift ( $\delta_H$ : 10-0.5 ppm), the classical carbohydrates ( $\delta_H \sim 3.4-4.1$  ppm) including methoxy peaks ( $\delta_H \sim 3.65$  ppm) declined from upper to deep layers (Figures 2-a3, 2-b3). The bioavailable carbohydrates in the chlorophyll maximum zone at the edge of the ACE (L05\_80 m) were more abundant than in the core (L11\_90 m) (Figure S4). In line with the supposed biological origin of olefins ( $H/C=C-$ ) (Hertkorn et al., 2013; Pisani et al., 2018), the relative abundance of olefinic protons in L05\_80 m was higher than in L11\_90 m (Figure S4). Here, lower nutrient availability at the core of the ACE could have attenuated photosynthetic and bacterial phytoplankton (Lasternas et al., 2013). In L11 station, the weight percentage of nitrogen (N%) decreased in the deep euphotic layer ( $\sim 200$  m) (Table 1), probably related to the fast recycling and remineralization of N-rich DOM by heterotrophs (Kujawinski, 2011) in SCS, where phytoplankton growth was limited by nitrogen availability (Chen et al., 2007). An analogous deficit of nitrogen content was not observed in L05 station, which could be explained by the addition of nutrients from the small-scale hotspot upwelling parts at the edge of the ACE (Samuelson et al., 2012). The increase of C/S ratio at the chlorophyll

maximum zone was more apparent in L05 station (211) (Table 1), indicating that depletion of sulfur was much stronger at the edge than at the core of the ACE (Zhou et al., 2013).

Principal component analysis (PCA) derived from 0.01 ppm buckets of  $^1H$  NMR spectra indicated that SPE-DOM of L11 formed a more homogeneous group than SPE-DOM of L05 (Figure S9A), suggesting that organic matter inside the eddy was chemically less diverse, likely resulting from a limited exchange of DOM in ACE with outside waters. PC1 represented more than half of influencing factors, with opposing horizontal ends indicating DOM in upper and deep layers, respectively. SPE-DOM in L11\_450 m was more similar to DOM in upper layers than L05\_400 m; possibly, downwelling in the ACE center had impact on DOM down to 450 m depth. The distribution of temperature, salinity and  $\sigma_t$  on section X also demonstrated a depth of eddy in excess of 450 m (Figure S1). In addition, the distribution of EEM-derived fluorescence components (discussed in supplementary material; Figure S10) as well as other bulk parameters of DOM (e.g. DOC,  $\Sigma P/\Sigma H$ , A/C, M/C; discussed in supplementary material; Figures S11, S12, S13, S14; Tables S4, S5) on the section X provided properties of water masses within and at the edge of the ACE (Figure S11). The ACEs in SCS influenced the waters down to more than 500 m (Xiang et al., 2016; He et al., 2018), and even more than 2000 m (Zhang et al., 2016). For the absence of sampling between 450 m and 700 m at L11, the exact depth that was visibly influenced by downwelling in the ACE center remained undefined.

NMR-derived hierarchical cluster analysis (HCA) produced two groups for both L05 and L11, comprising an upper layers group ( $\leq 200$  m) and a deep layers group ( $\geq 400$  m) (Figures S9b, S9c). Within the former, the SPE-DOM at 200 m depth was distinct from the surface samples in agreement with previous work (Hertkorn et al., 2013) that had shown maximum primary production at fluorescence maximum (L05\_80 m/L11\_90 m) whereas the surface sample (5 m) was affected by photodegradation.

FTICR/MS-derived HCA produced four groups in L05, discriminating upper layers (5 m and 80 m), mesopelagic zones (400 m and 1000 m), top mesopelagic layer (200 m) and deep layer (1898 m), whereas only two groups (upper layers  $\leq 200$  m and deep layers  $\geq 450$  m) were distinguished within L11 (Figures 3-a1, 3-a2). This indicated more distinctive differences of organic matter composition in the water profile at the edge of the eddy than at the center. FTICR/MS-derived HCA demonstrated that while in L05, small molecules ( $< 350$  Da) were more abundant in the upper and in the mesopelagic layers (Figures 3-b2, 3-c2), large molecules ( $> 450$  Da) were more abundant in the deep layers (Figure 3-e2). However, both small and large molecules were observed at 200 m depth (Figure 3-d2). The synchronicity of molecular distributions in analogous depth zones could be explained by analogous relationships of DOM production and degradation. In L11, comparative HCA-based analysis of mass spectra for surface and deep waters led to a remarkable discrimination: a tight cluster of rather unsaturated ( $H/C$ : 0.9-1.4) compounds from 300-470 Da was abundant at depth (Figure 3-g2) whereas more saturated compounds ( $H/C$ :

1.0-1.7) of considerable mass range from 230-830 Da were abundant in surface waters (**Figure 3-f2**). Both sets were mutually exclusive, producing a characteristic “dent” in the mass-edited H/C diagram of the surface SPE-DOM (**Figure 3-f2**). CRAM was commonly distributed from surface to deep (**Figure 3**), somewhat enriched in the deep layers (**Figures 3-e3, 3-g3**), indicating refractory DOM contributed more to total DOM in the deep layers, also in accordance with  $^1\text{H}$  NMR spectra (**Figure 2-a5, b5**). Carbohydrates and tannin-like compounds were abundant in upper 200 m (**Figures 3-b3, d3, f3**), while the less oxygenated CHOS molecular series were more abundant mainly in the mesopelagic and deep layers (**Figure 3-e3**).

## Metabolites and Biogeochemical Organic Matter in ACE of SCS

All  $^1\text{H}$  NMR spectra of L05 and L11 SCS SPE-DOM, including those in deep layers of water, showed a multitude of intense sharp NMR resonances, especially for  $\text{C}_{\text{sp}2}\text{H}$  units and within a narrow range of aliphatic protons from  $\delta_{\text{H}}$  0.9-1.5 ppm (**Figures 2, 4, 5, S2, S3**; cf. Chemical Diversity of SPE-DOM in SCS). These represented relatively abundant small molecules of putative biological (metabolites) or anthropogenic (pollutants) origin. Admitting a limited availability of meaningful NMR data (Hertkorn et al., 2013; Arakawa et al., 2017; Gonsior et al., 2017; Powers et al., 2019),  $^1\text{H}$  NMR spectra of typical PPL-based SPE-DOM isolated from mesopelagic and lower oceanic waters commonly display common broad bulk envelopes with rather marginal fine structure. Attenuation of sharp NMR resonances in  $^1\text{H}$  NMR spectra of methanolic solution of open ocean SPE-DOM arises from the presence of millions of atomic

environments (Hertkorn et al., 2008) in a highly processed biogeochemical material (cumulative projection of Lorenzian lines with finite line width onto NMR spectra with a limited overall bandwidth) which distribute in highly functionalized, oxygen- and often carboxyl-rich molecules (Hertkorn et al., 2006). This considerable functionalization facilitates mutual interactions between DOM molecules in solution, causing acceleration of transverse NMR relaxation and line broadening (Hertkorn, 2014), further lowering disposable S/N ratio and observability of concerned  $^1\text{H}$  NMR resonances. In contrast, photochemical degradation of isolated Pacific and Atlantic Ocean surface water in the lab had produced a suite of  $\sim 2\%$  polyols within hours which showed sharp NMR resonances and distinctive cross peaks in 2D NMR spectra (Gonsior et al., 2014). In SCS SPE-DOM, the relative abundance of analogous sharp NMR resonances was particularly pronounced in SPE-DOM L05\_1000 m, sufficient to produce a remarkable distinction in the visual appearance of its  $^1\text{H}$  NMR spectrum (**Figures 2, 5, S2, S3**), in NMR-derived HCA, and, particularly strong, in PCA (**Figure S9**). The large S/N ratio of the intense sharp NMR resonances in the 1D  $^1\text{H}$  NMR spectrum of L05\_1000 m relatively attenuated the (otherwise dominant) broad signature of common organic matter (**Figure S2**). The  $^1\text{H}$  NMR spectrum of SPE-DOM L05\_1000 m showed an array of  $\sim 15$  very and  $\sim 20$  less intense singlet resonances at  $\delta_{\text{H}} \sim 0.9\text{-}1.5$  ppm (**Figures 4, 5, S15A1, S16A1**) and strong NMR resonances in the aromatic region from  $\delta_{\text{H}} \sim 6.6\text{-}7.6$  ppm (**Figures 2, 5**). The most abundant aromatic compound showed J-coupling patterns characteristic of a 1,2,4-substituted benzene of which the upfield proton at  $\delta_{\text{H}} \sim 6.6$  ppm showed a single vicinal coupling  $^3J_{\text{HH}} \sim 7.5$  Hz (H6 in **Figures 5, S15A1, S16A1**), suggesting an adjacent oxygen atom in ortho-position. The

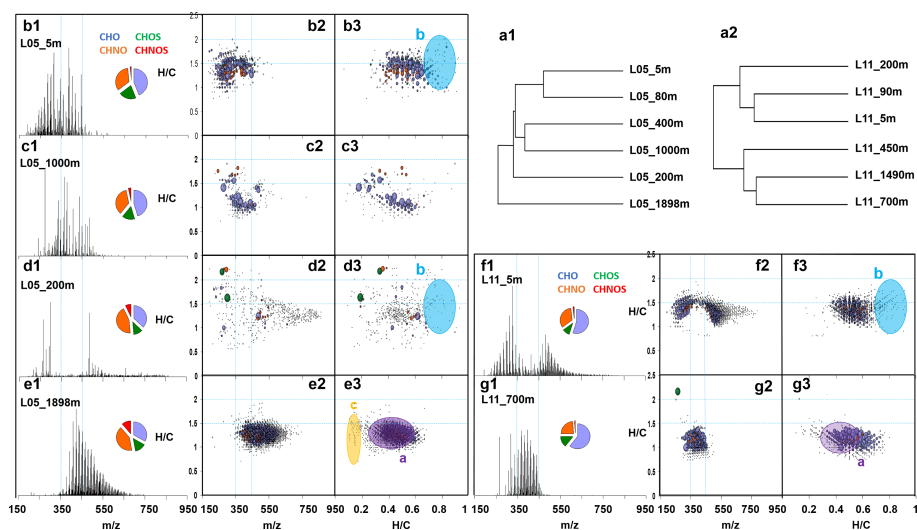


**FIGURE 3** | Comparative analysis of intensity weighted negative ESI FTICR mass spectra of marine SPE-DOM in stations L05 and L11 produced hierarchical cluster analysis (HCA) diagrams (a1, a2). From top to bottom rows: FTICR mass spectra from  $m/z$  150-950 with the assigned molecular compositions and relative proportions of color coded CHO (blue), CHOS (green), CHNO (orange) and CHNOS (red) molecular series, shown as van Krevelen diagrams and mass edited H/C ratios of the relatively more abundant compositions found in near surface layers (L5\_5m and L5\_80m) (b1-b3), mesopelagic layers (L5\_400m and L5\_1000m) (c1-c3), top mesopelagic layer (L5\_200m) (d1-d3), L05 deep (e1-e3), upper layers (L11\_5m, L11\_90m and L11\_200m) (f1-f3), and deep layers (L11\_450m, L11\_700m and L11\_1490m) SPE-DOM. Section a: CRAM; section b: Carbohydrates and tannin-like compounds; section c: Less oxygenated CHOS molecular series.

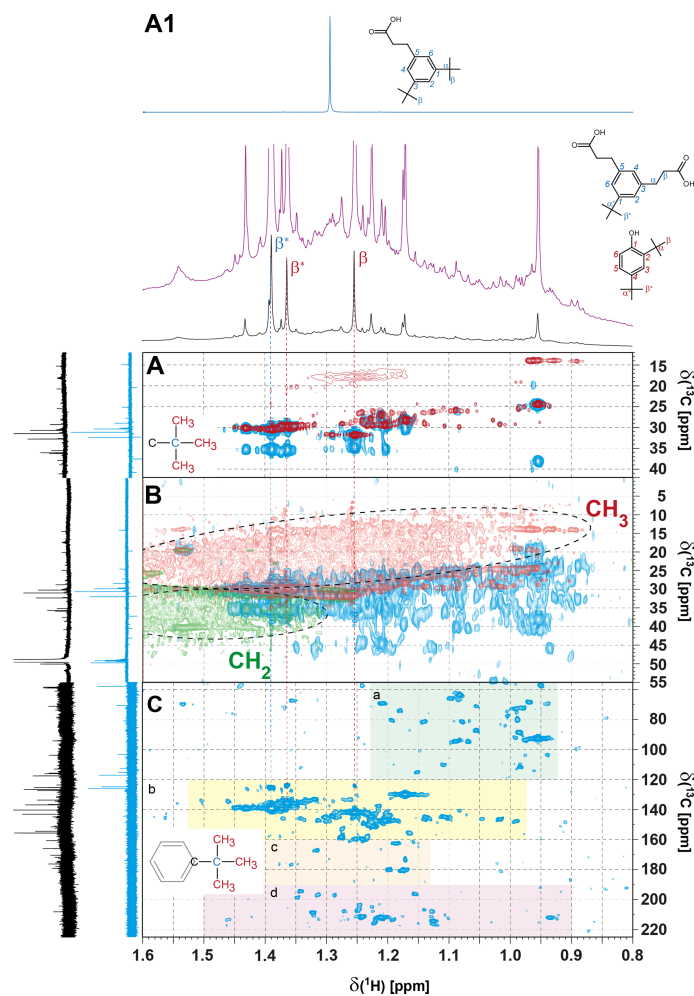


**FIGURE 4** |  $^1\text{H}$  NMR detected NMR spectra of  $\text{CCCH}_3$  groups of L05\_1000m SPE-DOM; **(A)**: most intense NMR cross peaks indicative of tert-butyl containing abundant molecules, with cross peaks from  $^1\text{H}$ ,  $^{13}\text{C}$  DEPT-HSQC NMR spectra in red and those of  $^1\text{H}$ ,  $^{13}\text{C}$  HMBC in blue color; **(B)**:  $^1\text{H}$ ,  $^{13}\text{C}$  DEPT-HSQC (red:  $\text{CH}_3$ ; green  $\text{CH}_2$ ) and  $^1\text{H}$ ,  $^{13}\text{C}$  HMBC (blue) NMR spectra of L05\_1000m SPE-DOM, shown down to lower cross peak amplitude; the common, contiguous cross peaks of biogeochemical organic matter show up in this display labelled by ellipsoids (cf. **Figures S15, S16**); **(C)**:  $^1\text{H}$ ,  $^{13}\text{C}$  HMBC cross peaks (blue color) represent common aliphatic branching motifs of DOM and relatively abundant molecules with considerable extent of aliphatic branching as exemplified by  $\delta_{\text{C}}$  ranging down to  $\delta_{\text{C}} \sim 55$  ppm ( $\text{CCCH}$  units). **(C)**:  $^1\text{H}$ ,  $^{13}\text{C}$  HMBC cross peaks (blue color) demonstrating abundance of aromatic compounds ( $\text{C}_{\text{ar}}\text{H}$  and  $\text{C}_{\text{ar}}\text{O}$  units;  $\delta_{\text{C}} \sim 120$ –160 ppm), a few carboxylic acids ( $\delta_{\text{C}} \sim 165$ –185 ppm), and several ketones ( $\delta_{\text{C}} \sim 195$ –220 ppm). Some of these units could represent to benzylic units of general character  $\text{C}_6\text{H}_x\text{Z-C}\alpha(\text{CH}_3)_n\text{-Y}_{3-n}$  in which Z would represent aromatic substitution and Y oxygenated aliphatic and aromatic units, including carboxylic acids and ketones. The benzylic position  $\text{C}\alpha$  would not carry directly bound protons, and *tert.* butyl  $\text{C}_4\text{H}_9$  then represents the most basic unit of such benzylic position.  $^{13}\text{C}$  NMR spectra are  $^{13}\text{C}$  single pulse (black) and  $\text{CH}_2$ -selective (blue)  $^{13}\text{C}$  DEPT NMR spectra.

NMR integral of the large aliphatic singlet NMR resonances was  $\sim 10$ -fold compared with that of the (single) aromatic protons H3, H5 and H6 (**Figures 5, S15**), which therefore represented tert-butyl ( $\text{C}_4\text{H}_9$ ) rather than methyl ( $\text{CH}_3$ ) groups. This identification also conformed to the observed  $^1\text{H}$  NMR chemical shift of the singlet NMR resonances at  $\delta_{\text{H}} \sim 1.2 \pm 0.3$  ppm, because  $\text{C}_{\text{ar}}\text{-CH}_3$  groups would resonate at  $\delta_{\text{H}} > 2.1$  ppm. Furthermore, 2-D NMR spectra of L05\_1000 m provided remarkable richness in detail and aided in improving preliminary assignment proposals from the one-dimensional  $^1\text{H}$  spectra.  $^1\text{H}$ ,  $^1\text{H}$ -resolved (JRES) NMR spectra confirmed 1,2,4 substitution of benzene ( $^3J_{\text{HH}}$ ,  $^4J_{\text{HH}}$ ) and the singlet character of the main NMR resonances of aliphatic protons from  $\delta_{\text{H}}$

0.9–1.5 ppm (**Figure S15A**). Strong cross peaks in the section from  $\delta_{\text{H}} \sim 0.9$ –1.5 ppm were observed in  $^1\text{H}$ ,  $^{13}\text{C}$  HSQC NMR spectra at  $\delta_{\text{C}} \sim 26$  ppm (**Figure 4A**, red) and in  $^1\text{H}$ ,  $^{13}\text{C}$  HMBC NMR spectra at  $\delta_{\text{C}} \sim 35$  ppm (**Figure 4**, blue), again corroborating presence of tert-butyl groups in abundance. The  $^1\text{H}$ ,  $^{13}\text{C}$  HMBC cross peak at  $\delta_{\text{H/C}} 2.79$  and 2.55 ppm/ $\sim 175$  ppm was assigned to a  $\text{C}_{\text{ar}}\text{-CH-CH-COOH}$  unit (**Figure 4**). The combination of 1-D and 2-D NMR spectra showed the presence of two major molecules: 2,4-di-tert-butylphenol (**M1**;  $\text{C}_{14}\text{H}_{22}\text{O}$ ; NMR data in accordance with (Yoon et al., 2006)) and 3,3'-(3-tert-butylbenzene-1,5-diyl) dipropanoic acid (**M2**;  $\text{C}_{16}\text{H}_{22}\text{O}_4$ ), a not yet described compound; SciFinder July 2020) and their analogues, which comprised 15% of the total

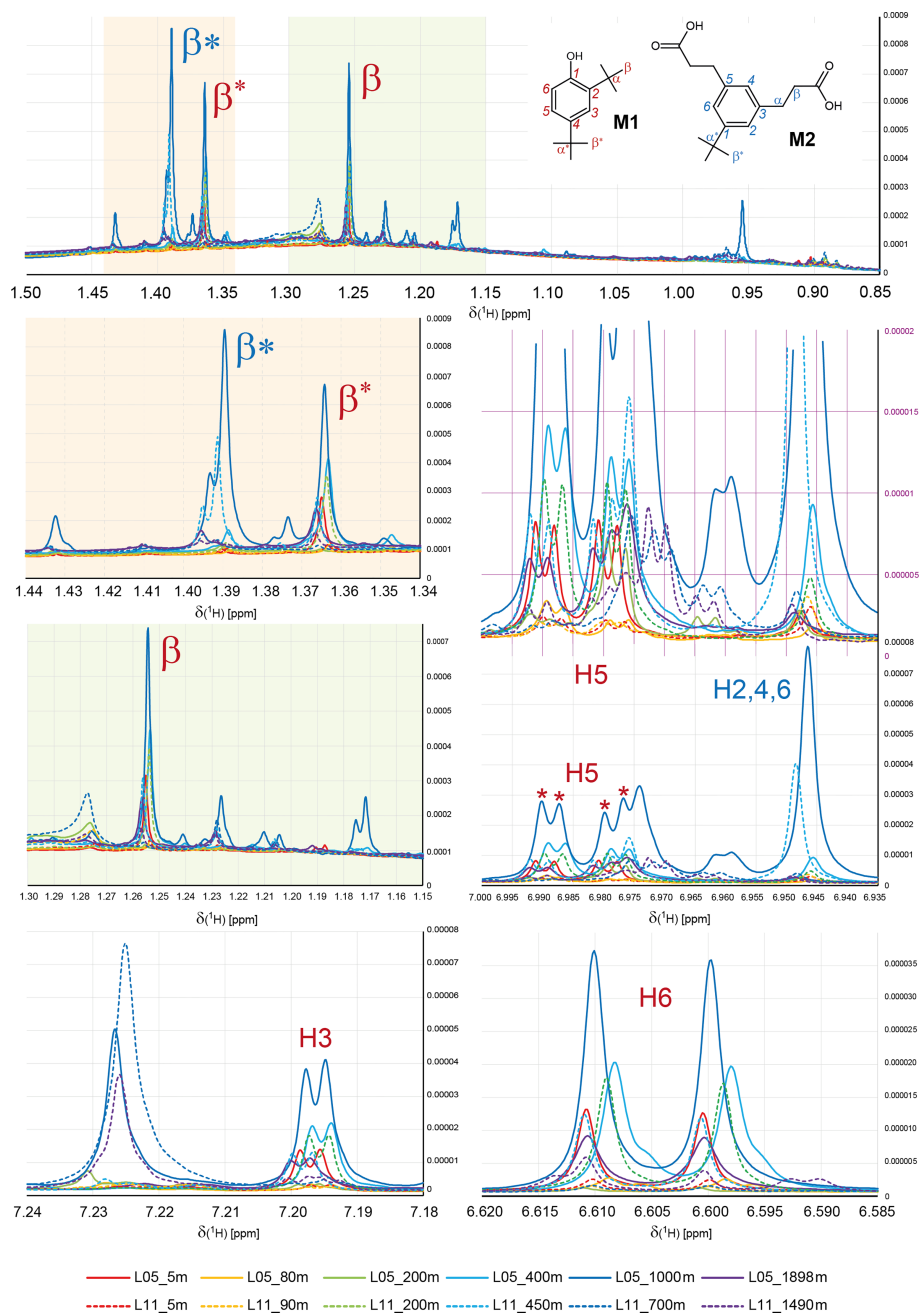


**FIGURE 5** | Area-normalized  $^1\text{H}$  NMR spectra (800 MHz,  $\text{CD}_3\text{OD}$ ; 0.5–10.0 ppm) of aliphatic and aromatic protons, demonstrating presence of the small molecules 2,4-di-*tert*-butylphenol (M1,  $\text{C}_{14}\text{H}_{22}\text{O}$ ; red) and 3,3'-(*tert*-butylbenzene-1,5-diyl)dipropionic acid (M2,  $\text{C}_{16}\text{H}_{22}\text{O}_4$ ; blue) at variable relative abundance in SCS SPE-DOM, with maximal relative abundance observed in SPE-DOM L05\_1000m (cf. text). The symbol "\*" under H5 indicates the NMR peaks of the hydrogen atom H5 on the aromatic ring of the M1 molecule.

$^1\text{H}$  NMR integral in L05\_1000 m (Figure S17). The relative abundance of compound M1 declined in the order L05\_1000 m > L05\_400 m > L11\_200 m > L5\_5 m  $\approx$  L11\_450 m > L5\_1898 m > L11\_1898 m > others, whereas that of M2 declined in the order L05\_1000 m > L11\_450 m > L5\_400 m > L5\_1898 m  $\approx$  L11\_700 m > others (Figure 5). Molecules M1 and M2 were

accompanied by about a dozen of compounds with similar  $^1\text{H}$  NMR properties (Figure 4), several of those showing *tert*-butyl groups as well, which frequently were connected to aromatic rings. The  $^1\text{H}$ ,  $^{13}\text{C}$  HMBC NMR spectrum of L05\_1000m presented remarkably strong cross peaks derived from ketones which very probably are marine derived natural products (Figures 4, S15).

*Tert*-butylphenols readily produce phenoxyl radicals and are used for stabilizing plastics; they are feedstock for the industrial synthesis of more complex antioxidants (Gerritsen et al., 1998; Remberger et al., 2004; Dhawan and Cholli, 2006; Yoon et al., 2006; Tollefsen et al., 2008; Zhang et al., 2013; Papa et al., 2014; Zhao et al., 2020). Additionally, they are found in inflows and effluents of municipal sewage treatment plants (Remberger et al., 2004). They also contribute to the endocrine disrupting potential in natural waters (Tollefsen et al., 2008), and are subject to bioaccumulation in fish (Papa et al., 2014) and other organisms (Gerritsen et al., 1998). The uptake, transformation and elimination within a food web depend on individual characteristics of organisms. In addition, 2,4-di-*tert*-butylphenol is a remarkably widespread metabolite of plants and bacteria also in the ocean (Chawawisit et al., 2015; Padmavathi et al., 2015), overall being produced by almost 200 species (Zhao et al., 2020). It shows a distinct potent broadband toxicity against almost all testing organisms, including the producing species itself (Zhao et al., 2020), and inhibits microbial quorum sensing *in vitro* (Chawawisit et al., 2015; Padmavathi et al., 2015). Photochemical  $\alpha$ -cleavage of di-*tert*-butylketone in the presence of phenols leads to ortho-, para-*tert*-butylphenols, and *t*-butyl phenyl ethers (Galindo et al., 1998). *Tert*-butylbenzene was a key oil contamination, which could be degraded by bacteria in deep water (Hazen et al., 2010; Lu et al., 2012). Bergauer et al. (2018) indicated that carboxylic acids could be one of essential substrates for the microbial community in the bathypelagic, and aromatic compounds were more likely to become utilized by heterotrophic prokaryotic community. The observed depth distribution of compounds **M1**, **M2** and associated molecules (**Figures 2, 5, S2, S3, S17**) was remarkable because relative proportions were maximal at meso- and bathypelagic depths and significantly exceeded near surface concentrations; specifically, **M1** and **M2** were virtually absent in the chlorophyll fluorescence maximum of both sampling stations L05\_80 m and L11\_90 m. Such specific low molecular weight phenols and carboxyl aromatics have not been previously reported in deep marine waters (1000 m), suggesting possible intermediate products in microbial food webs. Further studies are essential to demonstrate whether the abundance of **M1** and **M2** at the meso- and bathypelagic depths is related to the mesoscale eddies.

$^1\text{H}$ ,  $^1\text{H}$  COSY NMR spectra of marine SPE-DOM isolated from waters with high biological activity are very rich in detail and depict atomic environments of hundreds of organic molecules (Hertkorn et al., 2013). Common COSY cross peaks in marine DOM originate from relative abundant molecules, and direct comparison of those information-rich NMR spectra allows assessment of relative similarities and deviations of putative biological production in different ocean waters. It was therefore instructive to compare  $^1\text{H}$ ,  $^1\text{H}$  COSY NMR spectra of SCS SPE-DOM L05\_1000m with that of another previously recorded marine system, Atlantic Ocean fluorescence maximum SPE-DOM obtained at 48m depth (**Figures 6** and **Figure S18**).  $^1\text{H}$ ,  $^1\text{H}$  TOCSY NMR spectra with short mixing time (e.g. 15 ms) reveal short range J-coupled spin systems ( $^2/3J_{\text{HH}}$ ) alike  $^1\text{H}$ ,  $^1\text{H}$  COSY NMR spectra, but with substantially

higher sensitivity (Hertkorn, 2014) making these an obvious choice because only limited quantities of SPE-DOM L05\_1000m were available. (Bruch, 1996; Keeler, 2011).

Gonsior et al. (2014) observed very similar  $^1\text{H}$  NMR spectra of Atlantic and Pacific surface ocean SPE-DOM, indicative of common features governing the formation and degradation of highly processed biogeochemical DOM in these open ocean waters. In contrast, comparison of SPE-DOM isolated from Atlantic Ocean fluorescence maximum and South China Sea L05\_1000m waters revealed presence of fundamentally different but rather abundant organic molecules, in particular referring to aliphatic OCH and CCH units (**Figures 6, S18**). While both samples showed a higher relative concordance of their aromatic  $\text{C}_{\text{ar}}\text{H}$  units, distinction of cross peaks was visible as well in the major sections with electron withdrawing substitution, polycyclic aromatic hydrocarbons and six-membered N-heterocycles ( $\delta_{\text{H}} > 7.3$  ppm), in the sections of  $\text{C}_{\text{ar}}\text{H}$  with neutral ( $\delta_{\text{H}} \sim 7\text{--}7.3$  ppm) and electron donating substitution, as well as olefins and five membered heterocycles ( $\delta_{\text{H}} < 7$  ppm) (**Figures 6A, C**). The two major molecules **M1** (2,4-di-*tert*-butylphenol) and **M2** (3,3'-(3-*tert*-butylbenzene-1,5-diyl)dipropanoic acid) showed a few, not too influential strong cross peaks for  $\text{C}_{\text{ar}}\text{H}$  units while *tert*-butyl groups did not show appreciable TOCSY cross peaks from long range couplings (**Figure S15B**). The main distinction of both samples resided in the oxygenated aliphatic groups (OCH and OCCH units) and in the functionalization of aliphatic carboxylic acids; the latter were much more abundant and chemically diverse in SCS L05\_1000m than in Atlantic Ocean FMAX SPE-DOM. Carbohydrate-type OCH cross peaks ( $-\text{OCH}-\text{OCH}$  units, and alkylated carbohydrates:  $-\text{OCH}-\text{CH}$  units) were much more abundant in Atlantic Ocean FMAX SPE-DOM, suggesting earlier stages of organic matter production than observed in SCS L05\_1000m SPE-DOM. Here, *tert*-butyl derivatives of carboxylic acids were likely contributors to some but not to the majority of these TOCSY cross peaks ( $\text{HOOC}-\text{C}\alpha\text{H}-\text{C}\beta\text{H}-\text{Z}$  units; with Z including remote *tert*-butyl groups  $\text{C}_4\text{H}_9$ ).

Taking the bulk parameter DOC of SCS samples into consideration, the total concentration of these specific compounds **M1** and **M2** as computed from  $^1\text{H}$  NMR integrals (ratio of compound  $^1\text{H}$  NMR integral to total  $^1\text{H}$  NMR integral of SPE-DOM multiplied by DOC concentration) was maximal ( $\sim 6 \mu\text{mol L}^{-1}$ ) in L05\_1000 m, compared with the other depths. Such high abundance of putatively bioactive compounds at meso- and bathypelagic depths in SCS waters is truly remarkable. Since **M1** and **M2** were virtually absent in the chlorophyll fluorescence maximum of both the SCS water SPE-DOM (L05\_80 m and L11\_90 m), and the Atlantic Ocean water SPE-DOM (at 48 m), the enrichment of **M1** and **M2** in deep waters revealed the prominent effect of eddy on the production and depth distribution of these marine metabolites. Such production of such “unusual” molecules at depth has scarcely been reported, in part because only NMR spectroscopy provides straightforward access to these “unknown unknowns”. Most importantly, *tert*-butylphenols are endocrine disruptive compounds, with distinct potent broadband toxicity. These molecules may accumulate in organisms along the food chain and have long-term effects to marine system, not only in surface

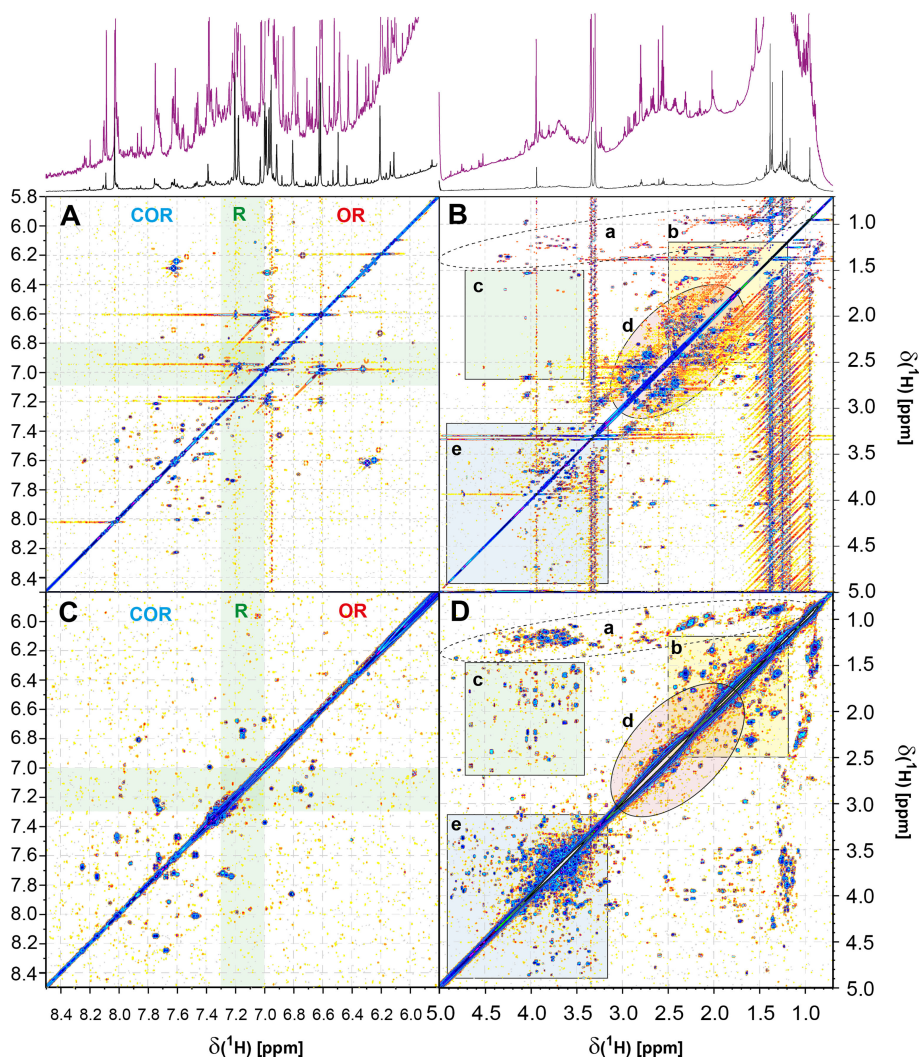


**FIGURE 6** | Homonuclear two dimensional  $^1\text{H}$ ,  $^1\text{H}$  NMR spectra and  $^1\text{H}$  NMR projection NMR spectra above of SCS L05\_1000 m SPE-DOM (**A, B**, TOCSY NMR with 15 ms mixing time) and of open Atlantic Ocean fluorescence maximum zone SPE-DOM at 48 m depth (**C, D**, COSY NMR spectrum) (Hertkorn et al., 2013) demonstrate considerable biomolecular diversity of these two marine DOM. NMR spectra indicate an earlier, carbohydrate-rich stage of organic matter processing following primary production in open Atlantic Ocean surface water, compared with that of South China Sea deep water, which is further oxidized showing a high proportion of carboxyl-rich alicyclic molecules CRAM (Hertkorn et al., 2006) (cf. text; for assignment of key substructures see the supporting online material).

but even in deep ocean waters (> 1000 m). Mesoscale marine chemical hotspots might induce chemotaxis of susceptible organisms (Raina et al., 2022) not only contributing to further processing of marine DOM but also influencing the productivity of marine ecosystems. In addition, physicochemical mechanisms of exporting unique molecules from and to meso- and bathypelagic depths are complex and ill constrained. Downwelling induced by ACE could penetrate down to 1000 m depth and residuals of unusual (bio)molecules could benefit from the “dilution effect” (Arrieta et al., 2015; Seidel et al., 2022). Zhang et al. (2014) observed deep-sea sediment transport processes driven by mesoscale eddies in the northern South China Sea at 2100 m water depth, close to our study zone, and deep-reaching eddies were shown to exert significant influence

on the settling velocity of marine snow and other particulates (Purkiani et al., 2020). Better understanding of TEP (transparent exopolymer particles) -mediated biogeochemical and ecological processes in deep oceans (Nagata et al., 2021) is needed. An enhanced understanding of lateral advection (from shelves, continents, or islands) and the dissolution from sinking particulate organic matter are other conceivable contributors of relevance (Seidel et al., 2022).

## CONCLUSION

Oceanic mesoscale eddies with horizontal scales of 50-300 km modulate the ocean biogeochemistry and are very influential in

the transport of heat, nutrients, DOC and other organic and inorganic compounds, and they play a decisive role in the confined South China Sea. While cyclonic eddies often inject nutrients from deep waters and thereby increase primary production in near surface waters, anticyclonic eddies (ACE) are characterized by downwelling at their core regime, with supposedly minor associated biogeochemical effects. While ACE-induced marine currents were not expected to fundamentally change the nature of its marine DOM as an extremely complex mixture of organic molecules, with all associated challenges of its molecular and structural analysis, a certain confinement of water masses on week-long time and kilometer size scales apparently decreased the overall molecular diversity of DOM of a depth profile from surface to bottom waters within an ACE, compared with the edge of an ACE. While small molecules of putative biological origin, such as 2,4-di-tert-butylphenol ( $C_{14}H_{22}O$ ) and 3,3'-(5-(tert-butyl)-1,3-phenylene) dipropionic acid ( $C_{16}H_{22}O_4$ ), were present in all waters, NMR spectroscopy enabled identification of specific tert-butyl derivatives at meso- and bathypelagic depths in single digit micromolar concentrations, and offered lead structures for other, yet unidentified olefinic and ketone-derived marine natural products. 2,4-di-tert-butylphenol could be a widespread product of marine algae and bacteria with potential for bioaccumulation within marine food webs, and associated toxicity for plentiful organisms. 3,3'-(3-tert-butylbenzene-1,5-diyl) dipropionic acid derived radicals could be the degraded by heterotrophic prokaryotic communities in the bathypelagic ocean, implying a potential contribution of microbial carbon pump in the marine system. Deviations from smooth mass peak distributions in FTICR mass spectra provided rather indirect evidence of biological processes associated with ACE, and mathematical analysis revealed alterations of biogeochemical processing at different positions and water depths. Active microbial metabolism across the entire water depth column in regions of up- and downwelling might create more abundant organic molecules than currently anticipated. Our study highlights the necessity to deciphering the structure and reactivity of marine organic molecules in a kinetic context, including the microbial and physicochemical constraints especially in the deep ocean (Gonsior et al., 2022).

These findings again emphasize the need for in-depth NMR spectral analyses for identification of “unknown unknowns” in marine waters, because FTICR mass spectrometry alone could not have produced significant lead information.  $^1H$  detected NMR spectroscopy could identify the structures of key molecules including quantification. Less superimposed 2D NMR spectra provided comprehensive information of key atomic chemical environments, demonstrating an active oceanic biogeochemistry of these unusual molecules. Future studies which combine investigation of spatially and temporally resolved microbial diversity, external (bulk) conditions and molecular features of DOM might select oceanic eddies as an attractive example for investigating the effect of intermediate size gradients on element, nutrient and molecule cycles. This will better constrain the relative proportions of biotic and abiotic interactions

governing the global carbon and other element cycles. These studies will propose relationships between groups of organisms and arrays of molecules, which allow testable predictions about biogeochemical processing in ocean waters.

## DATA AVAILABILITY STATEMENT

The original contributions presented in the study are included in the article/**Supplementary Material**. Further inquiries can be directed to the corresponding authors.

## AUTHOR CONTRIBUTIONS

MZ and YW contributed to the research design and sample collection. MZ, SL, and NH performed NMR acquisition, data analyses and interpretation. MZ, SL, and MH performed FTICR/MS acquisition and data analyses. PS–K provided support for the FTICR/MS analyses. DX provided the physical parameters. MZ, YW, SL, NH, and MH participated paper writing. All authors provided significant input on the final manuscript.

## FUNDING

The authors acknowledge the research funding provided by NSFC foundation (41876074), the National Program on Key Basic Research Project from the Ministry of Science and Technology of China (No. 2014CB441502), and the Research Funds of Happiness Flower ECNU (2021ST2110). We are thankful to the China Scholarship Council for the financial support of Miao Zhang (201806140082) and Siyu Li (201806360268).

## ACKNOWLEDGMENTS

The authors are grateful to our colleagues of State Key Laboratory of Estuarine and Coastal Research (SKLEC) (East China Normal University) as well as the Research Unit of Analytical Biogeochemistry (BGC) (Helmholtz Zentrum Munich). We appreciate the captain and crew in R/V *Nanfeng* during the sampling in March 2017. All data in this study are available in either tables in this manuscript and in the supporting information or upon request from the corresponding authors. The work has no real or perceived financial conflicts of interests for any author and affiliation.

## SUPPLEMENTARY MATERIAL

The Supplementary Material for this article can be found online at: <https://www.frontiersin.org/articles/10.3389/fmars.2022.902728/full#supplementary-material>

## REFERENCES

- Ali, D. A. B., and Tremblay, L. (2019). Hplc-SEC-FTIR Characterization of the Dissolved Organic Matter Produced by the Microbial Carbon Pump. *Mar. Chem.* 215, 103668. doi: 10.1016/j.marchem.2019.103668
- Andersson, A., Harir, M., Gonsior, M., Hertkorn, N., Schmitt-Kopplin, P., Kylin, H., et al. (2019). Waterworks-Specific Composition of Drinking Water Disinfection By-Products. *Environ. Sci.: Water Res. Tech.* 5 (5), 861–872. doi: 10.1039/C9EW00034H
- Arakawa, N., Aluwihare, L. I., Simpson, A. J., Soong, R., Stephens, B. M., and Lane-Coplen, D. (2017). Carotenoids are the Likely Precursor of a Significant Fraction of Marine Dissolved Organic Matter. *Sci. Adv.* 3 (9), e1602976. doi: 10.1126/sciadv.1602976
- Arnosti, C. (2011). Microbial Extracellular Enzymes and the Marine Carbon Cycle. *Ann. Rev. Mar. Sci.* 3, 401–425. doi: 10.1146/annurev-marine-120709-142731
- Arrieta, J. M., Mayol, E., Hansman, R. L., Herndl, G. J., Dittmar, T., and Duarte, C. M. (2015). Dilution Limits Dissolved Organic Carbon Utilization in the Deep Ocean. *Science* 348 (6232), 331–333. doi: 10.1126/science.1258955
- Baltar, F., Aristegui, J., Gasol, J. M., Lekunberri, I., and Herndl, G. J. (2010). Mesoscale Eddies: Hotspots of Prokaryotic Activity and Differential Community Structure in the Ocean. *ISME J.* 4 (8), 975–988. doi: 10.1038/ismej.2010.33
- Benner, R., and Amon, R. M. (2015). The Size-Reactivity Continuum of Major Bioelements in the Ocean. *Ann. Rev. Mar. Sci.* 7, 185–205. doi: 10.1146/annurev-marine-010213-135126
- Benner, R., Pakulski, J. D., McCarthy, M., Hedges, J. I., and Hatcher, P. G. (1992). Bulk Chemical Characteristics of Dissolved Organic Matter in the Ocean. *Science* 255 (5051), 1561–1564. doi: 10.1126/science.255.5051.1561
- Bergauer, K., Fernandez-Guerra, A., Garcia, J. A. L., Sprenger, R. R., Stepanauskas, R., Pachiadaki, M. G., et al. (2018). Organic Matter Processing by Microbial Communities Throughout the Atlantic Water Column as Revealed by Metaproteomics. *PNAS* 115 (3), E400–E408. doi: 10.1073/pnas.1708779115
- Bidigare, R. R., Benitez-Nelson, C., Leonard, C. L., Quay, P. D., Parsons, M. L., Foley, D. G., et al. (2003). Influence of a Cyclonic Eddy on Microheterotroph Biomass and Carbon Export in the Lee of Hawaii. *Geophys. Res. Lett.* 30 (6), 1318. doi: 10.1029/2002GL016393
- Broggi, S. R., Ha, S.-Y., Kim, K., Derrien, M., Lee, Y. K., and Hur, J. (2018). Optical and Molecular Characterization of Dissolved Organic Matter (DOM) in the Arctic Ice Core and the Underlying Seawater (Cambridge Bay, Canada): Implication for Increased Autochthonous DOM During Ice Melting. *Sci. Total Environ.* 627, 802–811. doi: 10.1016/j.scitotenv.2018.01.251
- Bruch, M. (1996). *NMR Spectroscopy Techniques* (Boca Raton, USA: CRC Press). doi: 10.1201/9781482273311
- Chawawisit, K., Bhoopong, P., Phupong, W., and Lertcanawanichakul, M. (2015). Anti-MRSA Activity, Mode of Action and Cytotoxicity of 2, 4-Di-tert-butylphenol Produced by *Streptomyces* Sp. KB1. *J. Pharm. Sci.* 5 (3), 007–012.
- Chen, Y.-L. L., Chen, H.-Y., Lin, I.-I., Lee, M.-A., and Chang, J. (2007). Effects of Cold Eddy on Phytoplankton Production and Assemblages in Luzon Strait Bordering the South China Sea. *J. Oceanogr.* 63 (4), 671–683. doi: 10.1007/s10872-007-0059-9
- Dhawan, A., and Cholli, A. (2006). *Synthesis of Sterically Hindered Phenol Based Macromolecular Antioxidants* (U.S.: Google Patents).
- Dittmar, T., Koch, B., Hertkorn, N., and Kattner, G. (2008). A Simple and Efficient Method for the Solid-Phase Extraction of Dissolved Organic Matter (SPEDOM) From Seawater. *Limnol. Oceanogr.: Methods* 6 (6), 230–235. doi: 10.4319/lom.2008.6.230
- Doblin, M. A., Petrou, K., Sinutok, S., Seymour, J. R., Messer, L. F., Brown, M. V., et al. (2016). Nutrient Uplift in a Cyclonic Eddy Increases Diversity, Primary Productivity and Iron Demand of Microbial Communities Relative to a Western Boundary Current. *PeerJ* 4, e1973. doi: 10.7717/peerj.1973
- Ewart, C. S., Meyers, M. K., Wallner, E. R., McGillicuddy, D. J. Jr., and Carlson, C. A. (2008). Microbial Dynamics in Cyclonic and Anticyclonic Mode-Water Eddies in the Northwestern Sargasso Sea. *Deep-Sea Res. Pt. II* 55 (10–13), 1334–1347. doi: 10.1016/j.dsr2.2008.02.013
- Fernandez, C., Thyssen, M., and Denis, M. (2008). Microbial Community Structure Along 18oW (39oN–44.5oN) in the NE Atlantic in Late Summer 2001 (POMME Programme). *J. Mar. Sys.* 71, 46–62. doi: 10.1016/j.jmarsys.2007.06.003
- Flerus, R., Lechtenfeld, O., Koch, B. P., McCallister, S., Schmitt-Kopplin, P., Benner, R., et al. (2012). A Molecular Perspective on the Ageing of Marine Dissolved Organic Matter. *Biogeosci. Discuss.* 9 (6), 1935–1955. doi: 10.5194/bg-9-1935-2012
- Galindo, F., Miranda, M. A., and R.J.J.o.P. and Chemistry, P. A. (1998). Coupling of Phenoxy and Alkyl Radicals Derived From the Photolysis of Phenol/Ketone Pairs: An Intermolecular Approach to the photo-Claisen Rearrangement. *J. Photoch. Photobio. A.* 117 (1), 17–19. doi: 10.1016/S1010-6030(98)00313-X
- Garcia, H. E., Gordon, L. I. (1992). Oxygen Solubility in Seawater: Better Fitting Equations. *Limnol. Oceanogr.* 37 (6), 1307–1312. doi: 10.4319/lo.1992.37.6.1307
- Garçon, V. C., Oschlies, A., Doney, S. C., McGillicuddy, D., and Waniek, J. (2001). The Role of Mesoscale Variability on Plankton Dynamics in the North Atlantic. *Deep-Sea Res. Pt. II* 48 (10), 2199–2226. doi: 10.1016/S0967-0645(00)00183-1
- Gerritsen, A., van der Hoeven, N., and Pielaat, A. (1998). The Acute Toxicity of Selected Alkylphenols to Young and Adult *Daphnia Magna*. *Ecotoxicol. Environ. Saf.* 39 (3), 227–232. doi: 10.1006/eesa.1997.1578
- Gonsior, M., Hertkorn, N., Conte, M. H., Cooper, W. J., Bastviken, D., Druffel, E., et al. (2014). Photochemical Production of Polyols Arising From Significant Photo-Transformation of Dissolved Organic Matter in the Oligotrophic Surface Ocean. *Mar. Chem.* 163, 10–18. doi: 10.1016/j.marchem.2014.04.002
- Gonsior, M., Luek, J., Schmitt-Kopplin, P., Grebmeier, J. M., and Cooper, L. W. (2017). Optical Properties and Molecular Diversity of Dissolved Organic Matter in the Bering Strait and Chukchi Sea. *Deep-Sea Res. Pt. II* 144, 104–111. doi: 10.1016/j.dsr2.2017.01.003
- Gonsior, M., Powers, L., Lahm, M., and McCallister, S. L. (2022). New Perspectives on the Marine Carbon Cycle—The Marine Dissolved Organic Matter Reactivity Continuum. *Environ. Sci. Tech.* 56, 5371–5380. doi: 10.1021/acs.est.1c08871
- Hazen, T. C., Dubinsky, E. A., DeSantis, T. Z., Andersen, G. L., Piceno, Y. M., Singh, N., et al. (2010). Deep-Sea Oil Plume Enriches Indigenous Oil-Degrading Bacteria. *Science* 330 (6001), 204–208. doi: 10.1126/science.1195979
- Hertkorn, N. (2014). *Nmr Spectroscopy: A Versatile Tool for Environmental Research* (New York, USA: John Wiley & Sons).
- Hertkorn, N., Benner, R., Frommberger, M., Schmitt-Kopplin, P., Witt, M., Kaiser, K., et al. (2006). Characterization of a Major Refractory Component of Marine Dissolved Organic Matter. *Geochim. Cosmochim. Acta* 70 (12), 2990–3010. doi: 10.1016/j.gca.2006.03.021
- Hertkorn, N., Frommberger, M., Witt, M., Koch, B. P., Schmitt-Kopplin, P., and Perdue, E. M. (2008). Natural Organic Matter and the Event Horizon of Mass Spectrometry. *Anal. Chem.* 80 (23), 8908–8919. doi: 10.1021/ac800464g
- Hertkorn, N., Harir, M., Cawley, K. M., Schmitt-Kopplin, P., and Jaffé, R. (2016). Molecular Characterization of Dissolved Organic Matter From Subtropical Wetlands: A Comparative Study Through the Analysis of Optical Properties, NMR and FTICR/MS. *Biogeosciences* 13 (8), 2257–2277. doi: 10.5194/bg-13-2257-2016
- Hertkorn, N., Harir, M., Koch, B., Michalke, B., and Schmitt-Kopplin, P. (2013). High-Field NMR Spectroscopy and FTICR Mass Spectrometry: Powerful Discovery Tools for the Molecular Level Characterization of Marine Dissolved Organic Matter. *Biogeosciences* 10, 1583–1624. doi: 10.5194/bg-10-1583-2012
- Hertkorn, N., Ruecker, C., Meringer, M., Gugisch, R., Frommberger, M., Perdue, E. M., et al. (2007). High-Precision Frequency Measurements: Indispensable Tools at the Core of the Molecular-Level Analysis of Complex Systems. *Anal. Bioanal. Chem.* 389 (5), 1311–1327. doi: 10.1007/s00216-007-1577-4
- He, Q., Zhan, H., Cai, S., He, Y., Huang, G., and Zhan, W. (2018). A New Assessment of Mesoscale Eddies in the South China Sea: Surface Features, Three-Dimensional Structures, and Thermohaline Transports. *J. Geophys. Res.-Oceans* 123 (7), 4906–4929. doi: 10.1029/2018JC014054
- Hoffmann, K., Bienhold, C., Buttigieg, P. L., Knittel, K., Laso-Perez, R., Rapp, J. Z., et al. (2020). Diversity and Metabolism of Woeseiales Bacteria, Global Members of Marine Sediment Communities. *ISME J.* 14 (4), 1042–1056. doi: 10.1038/s41396-020-0588-4
- Igarza, M., Dittmar, T., Graco, M., and Niggemann, J. (2019). Dissolved Organic Matter Cycling in the Coastal Upwelling System Off Central Peru During an “El Niño” Year. *Front. Mar. Chem.* 6, 198. doi: 10.3389/fmars.2019.00198
- Karstensen, J., Schütte, F., Pietri, A., Krahmann, G., Fiedler, B., Grundle, D., et al. (2017). Upwelling and Isolation in Oxygen-Depleted Anticyclonic Modewater

- Eddies and Implications for Nitrate Cycling. *Biogeosciences* 14 (8), 2167–2181. doi: 10.5194/bg-14-2167-2017
- Keeler, J. (2011). *Understanding NMR Spectroscopy* (New York, USA: John Wiley & Sons).
- Kellerman, A. M., Kothawala, D. N., Dittmar, T., and Tranvik, L. J. (2015). Persistence of Dissolved Organic Matter in Lakes Related to its Molecular Characteristics. *Nat. Geosci.* 8 (6), 454. doi: 10.1038/ngeo2440
- Klein, P., and Lapeyre, G. (2009). The Oceanic Vertical Pump Induced by Mesoscale and Submesoscale Turbulence. *Ann. Rev. Mar. Sci.* 1, 351–375. doi: 10.1146/annurev.marine.010908.163704
- Koch, B., and Dittmar, T. (2006). From Mass to Structure: An Aromaticity Index for High-Resolution Mass Data of Natural Organic Matter. *Rap. Commun. Mass Spect.* 20 (5), 926–932. doi: 10.1002/rcm.2386
- Kolasinski, J., Kaehler, S., and Jaquemet, S. (2012). Distribution and Sources of Particulate Organic Matter in a Mesoscale Eddy Dipole in the Mozambique Channel (South-Western Indian Ocean): Insight From C and N Stable Isotopes. *J. Mar. Sys.* 96, 122–131. doi: 10.1016/j.jmarsys.2012.02.015
- Kujawinski, E. B. (2011). The Impact of Microbial Metabolism on Marine Dissolved Organic Matter. *Ann. Rev. Mar. Sci.* 3 (1), 567–599. doi: 10.1146/annurev-marine-120308-081003
- Lasternas, S., Piedeleu, M., Sangrà, P., Duarte, C. M., and Agustí, S. (2012). Carbon Fluxes Forced by Anticyclonic Mesoscale Eddies Generated by Islands at the Subtropical NE Atlantic Ocean. *Biogeosci. Discuss.* 9 (8), 10241–10283. doi: 10.5194/bgd-9-10241-2012
- Lasternas, S., Piedeleu, M., Sangrà, P., Duarte, C. M., and Agustí, S. (2013). Forcing of Dissolved Organic Carbon Release by Phytoplankton by Anticyclonic Mesoscale Eddies in the Subtropical NE Atlantic Ocean. *Biogeosciences* 10 (3), 2129–2143. doi: 10.5194/bg-10-2129-2013
- Lu, Z., Deng, Y., Van Nostrand, J. D., He, Z., Voordeckers, J., Zhou, A., et al. (2012). Microbial Gene Functions Enriched in the Deepwater Horizon Deep-Sea Oil Plume. *ISME J.* 6 (2), 451–460. doi: 10.1038/ismej.2011.91
- Martínez-Pérez, A. M., Nieto-Cid, M., Osterholz, H., Catalá, T. S., Reche, I., Dittmar, T., et al. (2017). Linking Optical and Molecular Signatures of Dissolved Organic Matter in the Mediterranean Sea. *Sci. Rep.* 7 (1), 3436. doi: 10.1038/s41598-017-03735-4
- McGillicuddy, D. J. Jr (2016). Mechanisms of Physical-Biological-Biochemical Interaction at the Oceanic Mesoscale. *Ann. Rev. Mar. Sci.* 8, 125–159. doi: 10.1146/annurev-marine-010814-015606
- Nagata, T., Yamada, Y., and Fukuda, H. (2021). Transparent Exopolymer Particles in Deep Oceans: Synthesis and Future Challenges. *Gels* 7 (3), 75. doi: 10.3390/gels7030075
- Nebbioso, A., and Piccolo, A. (2013). Molecular Characterization of Dissolved Organic Matter (DOM): A Critical Review. *Anal. Bioanal. Chem.* 405 (1), 109–124. doi: 10.1007/s00216-012-6363-2
- Ohno, T., He, Z., Sleighter, R. L., Honeycutt, C. W., and Hatcher, P. G. (2010). Ultrahigh Resolution Mass Spectrometry and Indicator Species Analysis to Identify Marker Components of Soil- and Plant Biomass-Derived Organic Matter Fractions. *Environ. Sci. Tech.* 44 (22), 8594–8600. doi: 10.1021/es101089t
- Padmavathi, A. R., Abinaya, B., and Pandian, S. K. (2014). Phenol, 2,4-Bis(1,1-Dimethylethyl) of Marine Bacterial Origin Inhibits Quorum Sensing Mediated Biofilm Formation in the Uropathogen *Serratia Marcescens*. *Biofouling* 30 (9), 1111–1122. doi: 10.1080/08927014.2014.972386
- Padmavathi, A. R., Bakkiyaraj, D., Thajuddin, N., and Pandian, S. K. (2015). Effect of 2, 4-Di-Tert-Butylphenol on Growth and Biofilm Formation by an Opportunistic Fungus *Candida Albicans*. *Biofouling* 31 (7), 565–574. doi: 10.1080/08927014.2015.1077383
- Papa, E., van der Wal, L., Arnot, J. A., and Gramatica, P. (2014). Metabolic Biotransformation Half-Lives in Fish: QSAR Modeling and Consensus Analysis. *Sci. Total Environ.* 470–471, 1040–1046. doi: 10.1016/j.scitotenv.2013.10.068
- Pisani, O., Gao, M., Maie, N., Miyoshi, T., Childers, D. L., and Jaffé, R. (2018). Compositional Aspects of Herbaceous Litter Decomposition in the Freshwater Marshes of the Florida Everglades. *Plant Soil* 423 (1–2), 87–98. doi: 10.1007/s11104-017-3495-3
- Powers, L. C., Hertkorn, N., McDonald, N., Schmitt-Kopplin, P., Del Vecchio, R., Blough, N. V., et al. (2019). Sargassum Sp. Act as a Large Regional Source of Marine Dissolved Organic Carbon and Polyphenols. *Glo. Biogeo. Cyc.* 33 (11), 1423–1439. doi: 10.1029/2019GB006225
- Purkiani, K., Paul, A., Vink, A., Walter, M., Schulz, M., and Haeckel, M. (2020). Evidence of Eddy-Related Deep-Ocean Current Variability in the Northeast Tropical Pacific Ocean Induced by Remote Gap Winds. *Biogeosciences* 17 (24), 6527–6544. doi: 10.5194/bg-17-6527-2020
- Raina, J. B., Lambert, B. S., Parks, D. H., Rinke, C., Siboni, N., Barumucci, A., et al. (2022). Chemotaxis Shapes the Microscale Organization of the Ocean's Microbiome. *Nature* 605. doi: 10.1038/s41586-022-04614-3
- Remberger, M., Kaj, L., Palm, A., Sternbeck, J., Kvernes, E., and Brorström-Lundén, E. (2004). *Screening Tertiary Butylphenols, Methylphenols, and Long-Chain Alkylphenols in the Swedish Environment* (Stockholm, Sweden: IVL Svenska Miljöinstitutet AB).
- Repeta, D. J. (2015). *Biogeochemistry of Marine Dissolved Organic Matter*. Hansell, D., and Carlson, C. Eds (Amsterdam, Netherlands: Academic Press, Elsevier) 21–63.
- Samuelson, A., Hjøllo, S. S., Johannessen, J. A., and Patel, R. (2012). Particle Aggregation at the Edges of Anticyclonic Eddies and Implications for Distribution of Biomass. *Ocean Sci.* 8 (3), 389–400. doi: 10.5194/os-8-389-2012
- Šantl-Temkiv, T., Finster, K., Dittmar, T., Hansen, B. M., Thyraug, R., Nielsen, N. W., et al. (2013). Hailstones: A Window Into the Microbial and Chemical Inventory of a Storm Cloud. *PLoS One* 8 (1), e53550. doi: 10.1371/journal.pone.0053550
- Sarma, V., Yadav, K., and Behera, S. (2019). Role of Eddies on Organic Matter Production and F-Ratios in the Bay of Bengal. *Mar. Chem.* 210, 13–23. doi: 10.1016/j.marchem.2019.01.006
- Schmitt-Kopplin, P., Gabelica, Z., Gougeon, R. D., Fekete, A., Kanawati, B., Harir, M., et al. (2010a). High Molecular Diversity of Extraterrestrial Organic Matter in Murchison Meteorite Revealed 40 Years After its Fall. *PNAS* 107 (7), 2763–2768. doi: 10.1073/pnas.0912157107
- Schmitt-Kopplin, P., Gelencsér, A., Dabek-Zlotorzynska, E., Kiss, G., Hertkorn, N., Harir, M., et al. (2010b). Analysis of the Unresolved Organic Fraction in Atmospheric Aerosols With Ultrahigh-Resolution Mass Spectrometry and Nuclear Magnetic Resonance Spectroscopy: Organosulfates as Photochemical Smog Constituents. *Anal. Chem.* 82 (19), 8017–8026. doi: 10.1021/ac101444r
- Seidel, M., Vemulapalli, S. P. B., Mathieu, D., and Dittmar, T. (2022). Marine Dissolved Organic Matter Shares Thousands of Molecular Formulae Yet Differs Structurally Across Major Water Masses. *Environ. Sci. Tech.* 56 (6), 3758–3769. doi: 10.1016/j.ecoenv.2007.10.006
- Siegel, D. A., Peterson, P., McGillicuddy Jr, D. J., S. Maritorena, S., and Nelson, N. B. (2011). Bio-Optical Footprints Created by Mesoscale Eddies in the Sargasso Sea. *Geophys. Res. Lett.* 38, L13608. doi: 10.1029/2011GL047660
- Tollefsen, K. -E., Eikvar, S., Finne, E. F., Fogelberg, O., and Gregersen, I. K. (2008). Estrogenicity of Alkylphenols and Alkylated Non-Phenolics in a Rainbow Trout (*Oncorhynchus mykiss*) Primary Hepatocyte Culture. *Ecotox. Environ. Saftey* 71, 370–383.
- Wagner, S., Jaffé, R., Cawley, K., Dittmar, T., and Stubbins, A. (2015). Associations Between the Molecular and Optical Properties of Dissolved Organic Matter in the Florida Everglades, a Model Coastal Wetland System. *Front. Chem.* 3. doi: 10.3389/fchem.2015.00066
- Wang, L., Huang, B., Laws, E. A., Zhou, K., Liu, X., Xie, Y., et al. (2018). Anticyclonic Eddy Edge Effects on Phytoplankton Communities and Particle Export in the Northern South China Sea. *J. Geophys. Res.-Oceans* 123 (11), 7632–7650. doi: 10.1029/2017JC013623
- Wang, G., Su, J., and Chu, P. C. (2003). Mesoscale Eddies in the South China Sea Observed With Altimeter Data. *Geophys. Res. Lett.* 30 (21), 2121. doi: 10.1029/2003GL018532
- Xiang, R., Fang, W., and Zhou, S.-Q. (2016). The Anticyclonic Circulation in the Southern South China Sea: Observed Structure, Seasonal Development and Interannual Variability. *J. Mar. Sys.* 154, 131–145. doi: 10.1016/j.jmarsys.2015.10.004
- Xiu, P., Chai, F., Shi, L., Xue, H., and Chao, Y. (2010). A Census of Eddy Activities in the South China Sea During 1993–2007. *J. Geophys. Res.-Oceans* 115 (C3), C03012. doi: 10.1029/2009JC005657
- Yoon, M.-A., Jeong, T.-S., Park, D.-S., Xu, M.-Z., Oh, H.-W., Song, K.-B., et al. (2006). Antioxidant Effects of Quinoline Alkaloids and 2,4-Di-Tert-

- Butylphenol Isolated From *Scolopendra Subspinipes*. *Biol. Pharma.l Bull.* 29 (4), 735–739. doi: 10.1248/bpb.29.735
- Zhang, L., Cai, G., and Eli, W. (2013). Synthesis and Characterization of Novel Liquid Ester-Phenolic Antioxidant Based on Dipentaerythritol. *Lubri. Sci.* 25 (3), 209–216. doi: 10.1002/lis.1203
- Zhang, Y., Liu, Z., Zhao, Y., Wang, W., Li, J., and Xu, J. (2014). Mesoscale Eddies Transport Deep-Sea Sediments. *Sci. Rep.* 4 (1), 1–7. doi: 10.1038/srep05937
- Zhang, Z., Tian, J., Qiu, B., Zhao, W., Chang, P., Wu, D., et al. (2016). Observed 3D Structure, Generation, and Dissipation of Oceanic Mesoscale Eddies in the South China Sea. *Sci. Rep.* 6, 24349. doi: 10.1038/srep24349
- Zhao, F., Wang, P., Lucardi, R. D., Su, Z., and Li, S. (2020). Natural Sources and Bioactivities of 2,4-Di-Tert-Butylphenol and Its Analogs. *Toxins (Basel)* 12 (35). doi: 10.3390/toxins12010035
- Zhou, K., Dai, M., Kao, S.-J., Wang, L., Xiu, P., Chai, F., et al. (2013). Apparent Enhancement of <sup>234</sup>Th-Based Particle Export Associated With Anticyclonic Eddies. *Ear. Planet. Sci. Lett.* 381, 198–209. doi: 10.1016/j.epsl.2013.07.039

**Conflict of Interest:** The authors declare that the research was conducted in the absence of any commercial or financial relationships that could be construed as a potential conflict of interest.

**Publisher's Note:** All claims expressed in this article are solely those of the authors and do not necessarily represent those of their affiliated organizations, or those of the publisher, the editors and the reviewers. Any product that may be evaluated in this article, or claim that may be made by its manufacturer, is not guaranteed or endorsed by the publisher.

Copyright © 2022 Zhang, Li, Hertkorn, Harir, Xu, Schmitt-Kopplin and Wu. This is an open-access article distributed under the terms of the Creative Commons Attribution License (CC BY). The use, distribution or reproduction in other forums is permitted, provided the original author(s) and the copyright owner(s) are credited and that the original publication in this journal is cited, in accordance with accepted academic practice. No use, distribution or reproduction is permitted which does not comply with these terms.